Palaeogeography, Palaeoclimatology, Palaeoecology 688 (2026) 113625

Contents lists available at ScienceDirect

Palaeogeography, Palaeoclimatology, Palaeoecology

journal homepage: www.elsevier.com/locate/palaeo

Carbonate U-Pb dating potential for chronostratigraphy – Insights from the Maastrichtian-Danian lacustrine Yacoraite Fm. (Salta Rift)

Marta Gasparrini [a,*], Damaris Montano [a], Richard Albert [b,c], Sébastien Rohais [d], Axel Gerdes [b,c], Andrea Ceriani [e]

[a] Earth Sciences Department, University of Milan, 20133 Milan, Italy
[b] Institute of Geosciences, Goethe University Frankfurt, 60438 Frankfurt am Main, Germany
[c] Frankfurt Isotope and Element Research Center (FIERCE), Goethe University Frankfurt, Frankfurt am Main, Germany
[d] IFP Energies nouvelles, 92852 Rueil-Malmaison, France
[e] Earth Sciences Department, Khalifa University of Science and Technology, Abu Dhabi P.O. Box 127788, United Arab Emirates

ARTICLE INFO

Editor: L Angiolini

Keywords:
Lacustrine carbonates
U-Pb geochronology
Chronostratigraphy
Dating potential
Favorable environments
Favorable carbonate types

ABSTRACT

U-Pb LA-ICPMS geochronology of depositional carbonates demonstrated to be a potential chronostratigraphic tool for poorly time-framed sedimentary successions. However, not all carbonates are dateable. Evaluating the dating potential requires establishing the age accuracy and precision of various sedimentary and early diagenetic carbonates precipitated from the same system. This is of prime importance to boost future chronostratigraphic studies based on U-Pb LA-ICPMS analyses.

The lacustrine Yacoraite Fm. (Maastrichtian-Danian, Salta rift, Argentina) was chosen to assess the dating potential of different co-precipitated carbonates, whose age was constrained by zircon U-Pb dating of interbedded ash layers. Results of analyses on 101 carbonate phases, including ooids microbialites and early cements, are presented. Criteria to discriminate preserved U-Pb depositional ages were proposed to construct a robust depositional age model. Statistical analysis of the preserved depositional ages and their relative uncertainties ($2\sigma_{ex}$) point towards two factors that have partially controlled the carbonate U-Pb dating potential: the mineralogy and carbonate type that in turn reflect the dominant precipitation processes (chemical, induced or mediated by microbial activity), and textures (grain/crystal size and primary pore network). The highest dating potential is displayed by the early calcite cements precipitated via chemical processes and composed of coarse crystals with no micropores. Conversely, ooids and microbialites, especially those composed of dolomite, have lower dating potential. Results from this study provide insights regarding the sequestration of U and Pb in lacustrine carbonates and encourage to preferentially target early diagenetic calcite cements to apply U-Pb LA-ICPMS geochronology for chronostratigraphic studies.

1. Introduction

Continental sedimentary successions are typically less complete and more poorly preserved than the marine record. These features challenge correlations between time-equivalent lateral facies and, at a broader scale, limit stratigraphy reconstruction in sedimentary basins. Traditionally, stratigraphic correlations in continental successions mainly relied on radiometric dating of volcanic material coeval with the sedimentary deposits or on relative dating based on their palaeontologic content (Rubidge et al., 2013; Ogg et al., 2016; Smith et al., 2017). However, volcanic units that bracket stratigraphy may not always be present, and index fossils needed for biostratigraphy are commonly sparse or absent in continental successions. Consequently, the correlations in continental successions often rely on sequence stratigraphy only (e.g. Deschamps et al., 2012, 2020), implying uncertainties inherent to the method and a lack of robust age control.

U-Pb carbonate geochronology has the potential to provide the timing of carbonate precipitation directly. However, this was initially limited by the large volumes of carbonate required, the low success rate, and the time-consuming analytical procedures of the available ID-TIMS

* Corresponding author.
E-mail addresses: marta.gasparrini@unimi.it (M. Gasparrini), damaris.montano@unimi.it (D. Montano), RichardAlbert@fierce.uni-frankfurt.de (R. Albert), sebastien.rohais@ifpen.fr (S. Rohais), gerdes@em.uni-frankfurt.de (A. Gerdes), andrea.ceriani@ku.ac.ae (A. Ceriani).

https://doi.org/10.1016/j.palaeo.2026.113625
Received 3 September 2025; Received in revised form 4 February 2026; Accepted 5 February 2026
Available online 10 February 2026
0031-0182/© 2026 Published by Elsevier B.V.

(isotope dilution-thermal ionization mass spectrometry) technique (Smith and Farquhar, 1989; Rasbury and Cole, 2009). The advent of U-Pb geochronology on carbonates in thin sections by LA-ICPMS (laser ablation-inductively coupled plasma mass spectrometry) opened the possibility of dating small (100 s of microns) samples and increased the dating success rate as the higher spatial resolution minimizes mixtures of low and high U/Pb domains of the sample (Li et al., 2014; Roberts and Walker, 2016). This, together with the recent advances in sample selection, screening techniques and reference standards (e.g. Drost et al., 2018; Guillong et al., 2020, 2024; Roberts et al., 2017, 2020; Hoareau et al., 2021; Rasbury et al., 2021, 2023), allowed generation of U-Pb age constraints on carbonates formed in a variety of settings. Since then, carbonate U-Pb geochronology by LA-ICPMS has been chiefly applied to post-depositional diagenetic phases, such as cements, to constrain fluid-flow and tectonic events (e.g. Mangenot et al., 2018; Walter et al., 2018; Cruset et al., 2020; Mottram et al., 2020; Looser et al., 2021; Pan et al., 2021; Yang et al., 2022; Roberts and Holdsworth, 2022; Bilau et al., 2023; Gasparrini et al., 2023, 2025; Madritsch et al., 2024; Rocca et al., 2024). A more limited number of studies investigated sedimentary and early diagenetic carbonates (i.e. *syn*-depositional phases) and provided ages consistent with biostratigraphic and radiometric constraints, therefore suitable for chronostratigraphic studies (Liivamägi et al., 2018; Frisch et al., 2019; Hopley et al., 2019; Scardia et al., 2019; Parrish et al., 2019; Woodhead and Petrus, 2019; Kurumada et al., 2020; Meinhold et al., 2020; Nicholson et al., 2020; Brigaud et al., 2021; Hoareau et al., 2021; Montano et al., 2021, 2022; Rochín-Bañaga et al., 2021, 2024; Środoń et al., 2022; Rasbury et al., 2023; Aguirre Palafox et al., 2024; Monchal et al., 2025). However, not all sedimentary and early diagenetic carbonates provide accurate and sufficiently precise ages for chronostratigraphic purposes. The approach is limited by the carbonate dating potential (function of age accuracy and precision) which depends on variable factors among which the mineralogy and the environmental conditions in which they precipitated (Smith et al., 1994; Sturchio et al., 1998; Kelly et al., 2003, 2006; Cole et al., 2004; McManus et al., 2006; Tribovillard et al., 2006; Rasbury and Cole, 2009; Lachniet et al., 2012; Drake et al., 2018; Reeder et al., 2000; Roberts et al., 2020; Rasbury et al., 2021, 2023; Miyajima et al., 2021). Despite the amount of research recently demonstrating the reliability of carbonate U-Pb geochronology to reconstruct depositional ages of sedimentary successions, to date no study has investigated the dating potential of different types of carbonates from the same sedimentary system, based on a statistically significant number of samples. This causes a lack of prediction criteria for the dating potential of the differently formed carbonates.

The Yacoraite Formation (Fm.), a Maastrichtian-Danian lacustrine succession from the Salta rift (NW Argentina), stands out as an ideal target for such purpose since it consists of different *syn*-depositional carbonates (microbialites, oncoids, ooids, cements) with various mineralogy (calcite, dolomite). This study focuses on one stratigraphic section of the Yacoraite Fm., that was not affected by burial heating and diagenetic overprints and for which the sedimentologic and stratigraphic framework is well established (e.g. Rohais et al., 2019; Deschamps et al., 2020; Montano et al., 2023). Concordant U-Pb age constraints from carbonate and ash layer zircon were obtained from this stratigraphic section, demonstrating the exceptional accuracy and preservation of carbonate depositional ages (Montano et al., 2022). Here, additional carbonate samples from the same section are analyzed for U-Pb geochronology; the results are treated statistically to illustrate possible prediction criteria of continental carbonate dating potential, paving the ground for further understanding and advances in this domain.

2. Geological setting

The Salta rift basin (NW Argentina; Fig. 1A) belongs to the Andean basin system where a group of extensional basins developed during the Mesozoic continental rifting of South America. Structural highs along the axis of the Salta-Jujuy paleohigh separate the southern branch of the Salta rift basin into the Alemania and Metán sub-basins (Fig. 1B; Carrera et al., 2006, 2009).

The Salta Group represents the rift sedimentary infill. It is subdivided into three sub-groups representing different stages of the rift evolution: the Pirgua (syn–rift phase), the Balbuena (sag phase) and the Santa Bárbara (post-rift phase) (Salfity and Marquillas, 1994). The Balbuena subgroup includes the Maastrichtian-Danian Yacoraite Fm. consisting of lacustrine to shallow marine mixed carbonate–siliciclastic deposits, that formed coevally with the main stage of rift thermal subsidence under

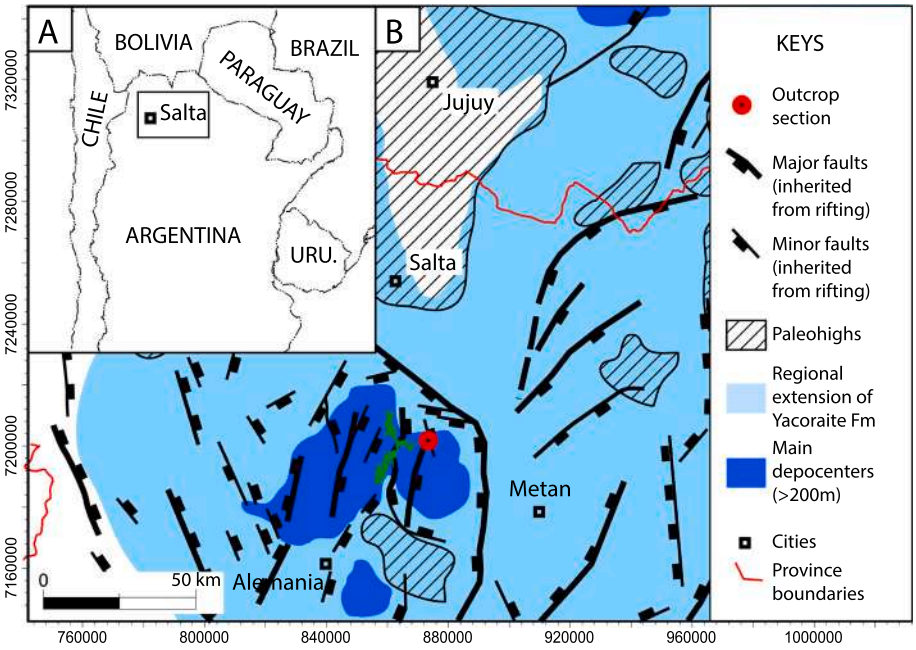

Fig. 1. *A. Salta* rift basin location in NW Argentina. B. Location of the Alemania and Metán sub-basins in the Salta Rift characterized by sag depocenters >200 m thick (modified from Romero-Sarmiento et al., 2019 and references therein). The studied stratigraphic section (red dot) outcrops in the vicinity of the Cabra Corral Lake (green area). (For interpretation of the references to colour in this figure legend, the reader is referred to the web version of this article.)

semi-arid climatic conditions (Salfity and Marquillas, 1994; Rohais et al., 2019; Deschamps et al., 2020; Gomes et al., 2020). The Yacoraite Fm. lithology includes shales, mudstones, oolitic packstones to grainstones and microbial boundstones, interbedded with fine- to coarse-grained sandstones (e.g. Marquillas, 1985; Salfity and Marquillas, 1994; Deschamps et al., 2020; Gomes et al., 2020; Villafañe et al., 2022; Mutti et al., 2023). Volcanic ash layers occur interbedded within the sedimentary succession and span ages from 67.55 ± 0.80 to 63.33 ± 0.56 Ma (Montano et al., 2022, 2023 and references therein).

The stratigraphic architecture of the Yacoraite Fm. is characterized by multiple hierarchies of cyclicity, primarily controlled by climate-derived parameters. The present study considers the mid-term cyclicity reported by Rohais et al. (2019) and Deschamps et al. (2020) for the Alemania and Metán sub-basins, where the Yacoraite Fm. is subdivided into four mid-term (third-order) stratigraphic sequences.

The Yacoraite Fm. in the Metán sub-basin did not experience significant heating during burial, as demonstrated by Rock-Eval and vitrinite reflectance data from the organic-rich fine deposits of the Cabra Corral Lake area (Fig. 1B), indicating that the kerogen remained in the immature to early-mature temperature window (Romero-Sarmiento et al., 2019). Indeed, most depositional and early diagenetic carbonates of the Yacoraite Fm. from this area preserve pristine geochemical features and were only locally overprinted by late diagenesis (Durieux and Brown, 2007). Consequently, the O and C isotope signatures of these carbonates have been used to reconstruct the lacustrine water composition (Sial et al., 2001; Marquillas et al., 2007; Rohais et al., 2019; Gomes et al., 2020; Montano et al., 2023; Mutti et al., 2023).

3. Available data and investigated samples

The investigated samples come from the 238 m thick Juramento stratigraphic section (e.g. Marquillas et al., 2007; Rohais et al., 2019; Deschamps et al., 2020), that crops out in the vicinity of the Cabra Corral Lake from the Metán sub-basin (Fig. 1B). This stratigraphic section is located close to one of the main depocenters and possibly lacks major hiatuses (>0.1 to 0.4 Ma) that instead characterize the more proximal domains (Deschamps et al., 2020). Several volcanic ash layers are interbedded with carbonate and siliciclastic facies along the section (Fig. 2A-B). These facies contain carbonate sedimentary material of different origins (e.g., stromatolites, ooids, oncoids) of calcitic and dolomitic mineralogy (Fig. 2) and early diagenetic calcite cements.

Detailed sedimentology and stratigraphy investigations of the Juramento section area were already undertaken at outcrops (Rohais et al., 2019; Deschamps et al., 2020; Teles et al., 2023) and led to the identification of 10 facies associations and corresponding depositional environments and to the establishment of five sequence boundaries (named SB1 to SB5 from base to top) separating four third-order stratigraphic sequences (Deschamps et al., 2020; Fig. 3A).

In total, six ash layers and 120 carbonate samples were collected along the Juramento section away from mineralized fractures and exposure surfaces to minimize potential modification of the carbonate pristine geochemistry by later diagenetic fluids. Detailed macro- and micro-facies characterization together with O-C stable isotope analyses of carbonates were also performed (Rohais et al., 2019; Deschamps et al., 2020; Montano et al., 2022, 2023; Fig. 3B). A robust depositional age model was reconstructed using zircon U-Pb dating from the ash layers and 13 carbonate samples were investigated for diagenetic characterization and LA-ICPMS U-Pb dating (Montano et al., 2022). This latter study demonstrated that U-Pb geochronology of *syn*-sedimentary material may give accurate and precise ages, allowing the reconstruction of a robust depositional age model that overlaps the one obtained from ash layer zircons (Fig. 3C; Montano et al., 2022).

In the present study we conducted petrographic characterization (micro-facies, diagenesis) and U-Pb dating on further 36 carbonate samples including different types of syn-depositional materials (i.e. microbialites, oncoids, ooids, early calcite cements).

4. Methodologies

4.1. Facies and diagenesis analyses

Polished thin sections (50–60 μm thick) were investigated by petrography and specifically for micro-facies and diagenesis analysis. Conventional optical microscopy was undertaken using a Nikon ECLIPSE LV100 POL polarized light microscope which allowed observations under plane-polarized light (PPL). Cathodoluminescence (CL) microscopy was undertaken with a CITL 8200 Mk5 cold CL instrument; the electron beam worked under vacuum (<0.1 mbar) with an acceleration voltage of 10 kV and a current of 250 μA. The thin sections were partially stained with a solution of 10% diluted HCl, Alizarin red-S and potassium ferricyanide (Dickson, 1966).

Carbonate textures were described using the Dunham (1962) classification, whereas facies and depositional environments were attributed to the scheme proposed by Deschamps et al. (2020). In this respect, the term stromatolite may include the microbial boundstone that.

will be here simply named microbialite and which microfabrics were described using the terminology of Riding (1991, 2000).

4.2. U-Pb geochronology

Polished thin sections were analyzed in 6 U-Pb LA-ICPMS analytical sessions. Before analysis, thin sections were cleaned in an ultrasonic bath with ethanol. During the LA-sessions, the ablation parameters were kept stable for all samples and reference materials. Thin sections were ablated in a helium atmosphere (300 ml/min) and mixed in the ablation funnel with argon (1 l/min) and nitrogen (6 to 8 ml/min). Analyses were performed with square ablation spots (213 μm × 213 μm), 8 Hz repetition rate and a fluence of about 2 J/cm^2. A manual pre-screening session was performed on all carbonate phases previously distinguished via microscopy investigation and allowed identifying areas with variable $^{238}U/^{206}Pb$ and $^{207}Pb/^{206}Pb$ ratios. On phases with isotopic ratio variations analyses were performed; the analyzed number of LA-spots (n) is variable (mean 25.0 ± 9.6) and depended also on the abundance of the target phases in thin section. The settings of the laser and the ICP-MS instrument are given in Appendix A (Supplementary Material).

Raw data were corrected offline using the Isoplot (Ludwig, 2012) supported by Microsoft Excel-based spreadsheet (Gerdes and Zeh, 2006, 2009). Fractionation of $^{238}U/^{206}Pb$, $^{207}Pb/^{206}Pb$ ratios and their drift were corrected based on repeated analyses of soda-lime glass NIST-SRM 614. WC-1 calcite RM (Roberts et al., 2017) was used to correct for the session-specific matrix offset (c. 5%, see Appendix A) between NIST glass and carbonate. Results were plotted in U-Pb Tera-Wasserburg Concordia diagrams and ages with internal uncertainties (2σ) were calculated as the lower intercept of the regression lines with the Concordia curve. Regression lines of the dateable carbonate phases were constrained with $13 < n < 46$ ablation spots (mean 24.7 ± 9.2). 2σ uncertainties were propagated to include systematic uncertainties ($2\sigma_{ex}$) and were calculated following Horstwood et al., 2016 (see Appendix A). The information about the RM can be also found in Appendix A. No common Pb corrections were applied and the long-term variance used is 1.5% (2σ; Montano et al., 2021).

5. Results and interpretations

As stated in section "2. Available data and investigated samples" the petrography/diagenesis and U-Pb geochronology of carbonates along the Juramento section were investigated in two different stages of data acquisition (Fig. 3A):

1) 13 samples including 23 carbonate phases (Montano et al., 2022);
2) 36 samples including 78 carbonate phases (present study).

This contribution mainly aims to identify the carbonate ages representative of the depositional event and treat them statistically to gain

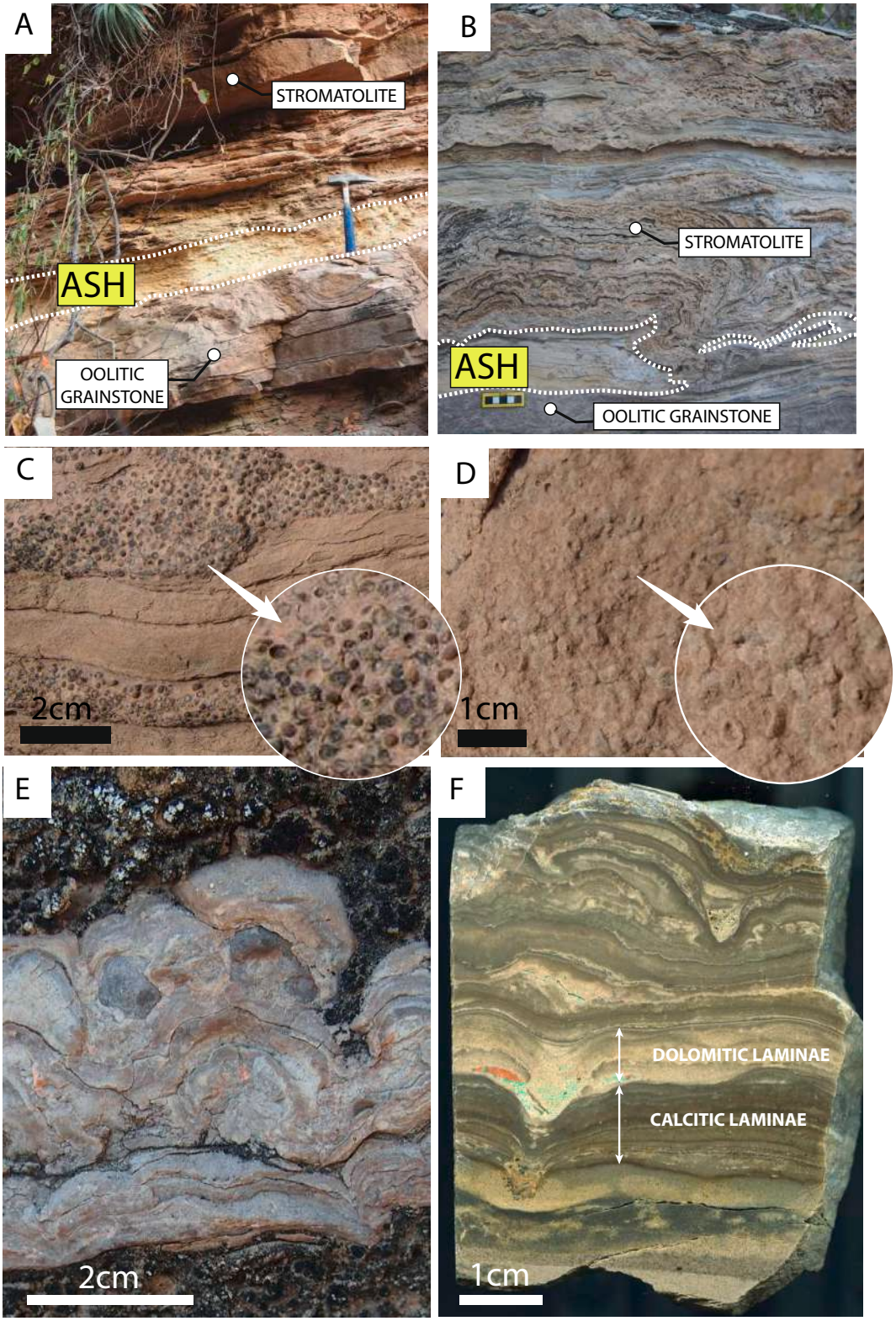

Fig. 2. A. and B. Field images of volcanic ash layers (highlighted by white dashed lines) occur interbedded within the sedimentary deposits. In A. the 20-cm thick tabular ash layer overlies oolitic grainstone (121 m from the base, Sequence 2). In B. planar laminated to moustache-like stromatolite growing into a lenticular ash layer at the top of the Juramento section (219 m from the base, Sequence 4). C. Field image of oolitic grainstone beds (UJ14 sample, Sequence 1). D. Field photograph of oncoidal rudstone (UJ20 sample, Sequence 1). E. Hand specimen of planar laminated to moustache-like stromatolite (UJ45 sample, Sequence 2). F. Hand specimen of planar laminated stromatolite with alternation of calcitic (grey) and dolomitic (beige) millimetric to sub-millimetric laminae (JURD3 sample, Sequence 4).

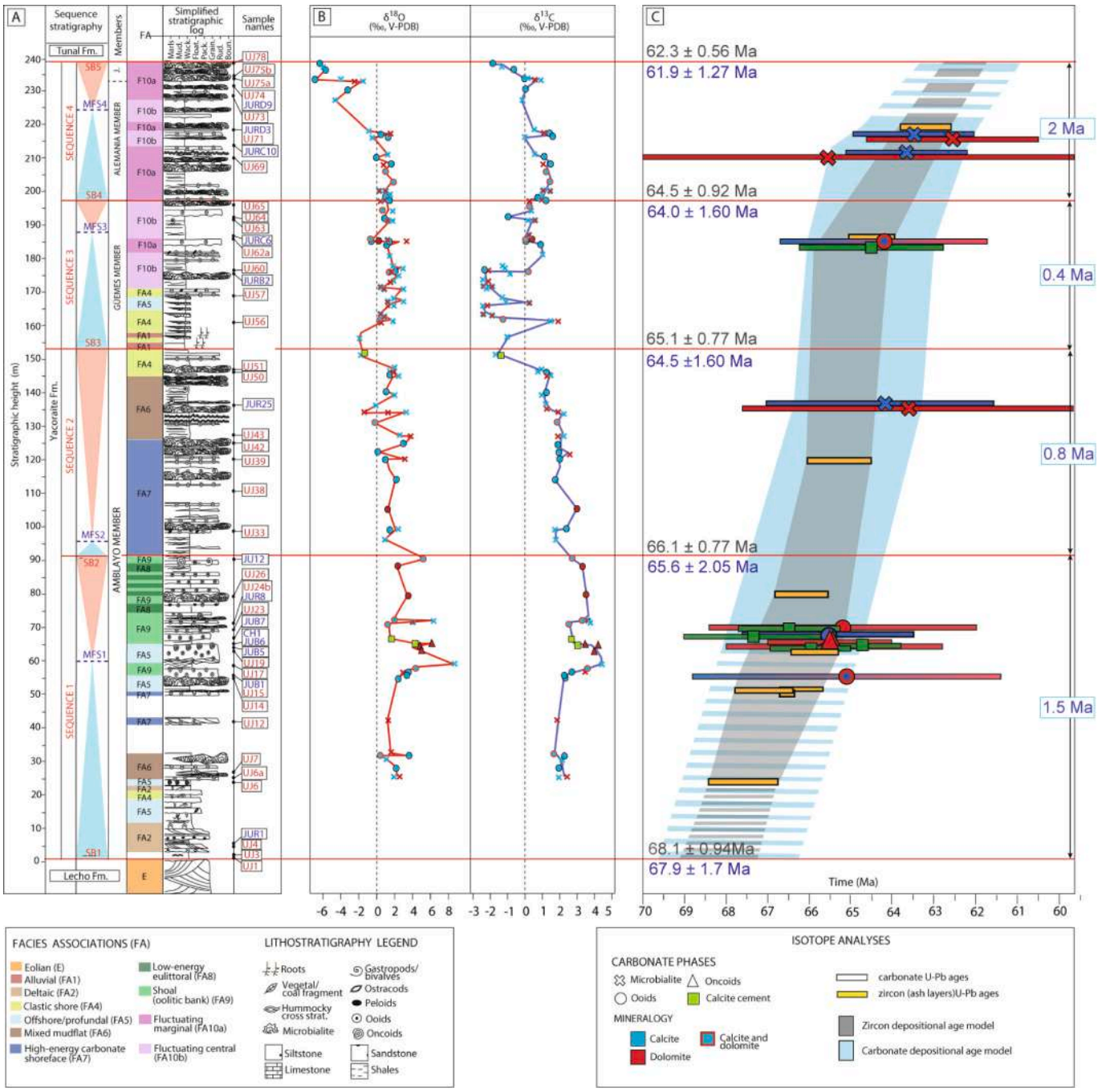

Fig. 3. Available data from the Yacoraite Fm. along the Juramento section. A. Stratigraphy, sedimentology, and sampling. The position of sequence boundaries (SB; red horizontal lines) is after Rohais et al. (2019) and Deschamps et al. (2020). Sample names refer to the carbonate samples investigated by U-Pb geochronology by Montano et al. (2022) in blue ($n = 13$) and in this study in red ($n = 36$). B. O-C stable isotope compositions for different carbonate phases after Montano et al. (2023). C. Depositional age models from zircon (grey area) and carbonate (blue area) U-Pb geochronology from Montano et al. (2022). Sequence boundary ages are reported in grey and blue if derived from zircon and carbonate depositional age models, respectively. In the blue frames is the duration of each stratigraphic sequence, inferred from the carbonate depositional age model. The reported age uncertainties are $2\sigma_{ex}$. (For interpretation of the references to colour in this figure legend, the reader is referred to the web version of this article.)

insights into the dating potential of different lacustrine carbonates for chronostratigraphy applications. Therefore, the data derived from the two analytical stages will be treated and presented together.

5.1. Petrography and U-Pb dating

Details on micro-facies characterization of the Yacoraite Fm. carbonates from the Juramento section can be found in previous literature (Deschamps et al., 2020; Montano et al., 2023). Here the thin section petrographic study mainly aimed to 1) identify different types of sedimentary carbonates and early diagenetic cements (i.e., the *syn*-depositional or syn-sedimentary carbonate phases); 2) select for U-Pb geochronology the carbonate phases that satisfy the criteria of preserved internal structures and lack of dissolution/recrystallization evidence (see Montano et al., 2021), and that therefore possibly preserved the pristine geochemical signature.

In total 101 syn-sedimentary carbonate phases from 49 samples were analyzed for U-Pb geochronology. Table 1 reports information about the

Table 1
U-Pb geochronology data obtained for the carbonate samples (n = 49) investigated. Carbonate phases (n = 101) are: calcitic microbialite (MIC-C), dolomitic microbialite (MIC-D), dolomitic oncoids (OND), calcitic ooids (OC), dolomitic ooids (OD), mixed calcitic-dolomitic ooids (OM) and early calcite cement (EC). The asterisk in the sample name column indicates the dated carbonate phases published by Montano et al. (2022). Undateable carbonate phases (n = 42) are those for which no U-Pb data are reported. U-Pb data of phases giving errorchrons (n = 7) are marked to strikethrough. The remaining phases (n = 52) were considered dateable.

Strat. height (m)	Sample name	Carbonate phase	Age (Ma)[1]	2σ (Ma)[2]	2σ (%)[3]	$2\sigma_{ex}$ (Ma)[4]	$2\sigma_{ex}$ (%)[5]	$^{207}Pb/^{206}Pb \pm 2\sigma$[6]	MSWD[7]	n[8]
238.0	UJ78	OC	~~37.54~~	~~22.24~~	~~59.23~~	~~22.24~~	~~59.25~~	~~0.815 ± 0.004~~	~~0.49~~	~~22~~
238.0	UJ78	MIC-C	–	–	–	–	–	–	–	–
235.0	UJ75b	OC	61.53	8.19	13.31	8.25	13.41	0.819 ± 0.002	0.57	30
235.0	UJ75b	MIC-C	–	–	–	–	–	–	–	–
234.0	UJ75a	MIC-C	~~69.04~~	~~18.81~~	~~27.24~~	~~18.85~~	~~27.30~~	~~0.813 ± 0.005~~	~~0.48~~	~~13~~
232.0	UJ74	OC	63.44	3.36	5.20	3.50	5.52	0.821 ± 0.003	0.56	20
231.5	JURD9*	OC	–	–	–	–	–	–	–	–
228.0	UJ73a	MIC-C	64.56	1.12	1.73	1.48	2.29	0.827 ± 0.003	0.52	25
228.0	UJ73b	MIC-C	63.54	1.37	2.15	1.67	2.63	0.828 ± 0.003	0.27	35
228.0	UJ73c	MIC-C	63.66	0.55	0.86	1.10	1.73	0.824 ± 0.002	1.38	30
228.0	UJ73	MIC-D	63.30	1.20	1.89	1.52	2.40	0.828 ± 0.003	0.70	28
218.5	JURD3*	MIC-C	63.44	1.53	2.40	1.80	2.84	0.820 ± 0.002	1.79	40
218.5	JURD3*	MIC-D	62.58	2.05	3.27	2.26	3.61	0.824 ± 0.003	0.82	18
218.0	UJ71	OC	61.95	5.33	8.60	5.41	8.73	0.821 ± 0.002	0.54	13
218.0	UJ71	MIC-C	–	–	–	–	–	–	–	–
213.5	JURC10*	MIC-C	63.66	1.44	2.26	1.73	2.72	0.825 ± 0.005	0.82	19
213.5	JURC10*	MIC-D	66.81	11.15	16.69	11.20	16.76	0.826 ± 0.007	0.61	13
210.0	UJ69	MIC-C	59.35	2.36	3.98	2.53	4.26	0.817 ± 0.005	2.09	23
210.0	UJ69	MIC-D	–	–	–	–	–	–	–	–
196.0	UJ65	MIC-D	–	–	–	–	–	–	–	–
196.0	UJ65	OM	–	–	–	–	–	–	–	–
196.0	UJ65	MIC-M	–	–	–	–	–	–	–	–
193.0	UJ64	OC	63.54	4.48	7.05	4.58	7.21	0.821 ± 0.004	0.16	25
193.0	UJ64	MIC-C	–	–	–	–	–	–	–	–
192.5	UJ63	MIC-C	~~174.29~~	~~101.33~~	~~58.14~~	~~101.40~~	~~58.18~~	~~0.837 ± 0.012~~	~~5.93~~	~~7~~
187.0	JURC6*	OM	64.25	2.48	3.86	2.66	4.14	0.823 ± 0.004	0.74	24
187.0	JURC6*	EC	64.51	1.73	2.68	1.98	3.07	0.811 ± 0.001	1.01	16
186.5	UJ62a	EC	62.36	1.15	1.84	1.48	2.37	0.818 ± 0.004	0.98	25
186.5	UJ62a	OC	54.44	3.64	6.69	3.74	6.87	0.810 ± 0.005	0.86	22
177.0	UJ60	MIC-C	64.44	1.64	2.55	1.91	2.96	0.823 ± 0.002	0.96	31
176.0	JURB2*	MIC-C	–	–	–	–	–	–	–	–
176.0	JURB2*	MIC-D	–	–	–	–	–	–	–	–
169.0	UJ57	OC	63.21	2.04	3.23	2.25	3.56	0.820 ± 0.003	0.64	29
169.0	UJ57	EC	–	–	–	–	–	–	–	–
161.0	UJ56	MIC-C	56.92	5.13	9.01	5.20	9.14	0.817 ± 0.006	1.01	24
161.0	UJ56	OC	–	–	–	–	–	–	–	–
161.0	UJ56	MIC-D	–	–	–	–	–	–	–	–
147.0	UJ51	MIC-C	64.13	2.21	3.45	2.41	3.76	0.823 ± 0.001	0.83	33
147.0	UJ51	MIC-D	–	–	–	–	–	–	–	–
146.0	UJ50	OC	66.17	3.53	5.33	3.67	5.55	0.817 ± 0.001	0.47	31
146.0	UJ50	MIC-C	63.41	3.64	5.74	3.77	5.95	0.817 ± 0.002	0.67	26
136.0	JUR25*	MIC-C	64.31	2.64	4.11	2.81	4.37	0.8258 ± 0.003	0.67	29
136.0	JUR25*	MIC-D	63.62	3.98	6.26	4.09	6.43	0.834 ± 0.005	1.58	22
127.0	UJ43	MIC-C	60.75	1.29	2.12	1.58	2.60	0.820 ± 0.004	0.87	28
127.0	UJ43	MIC-M	–	–	–	–	–	–	–	–
127.0	UJ43	OM	–	–	–	–	–	–	–	–
125.0	UJ42	OC	65.79	2.87	4.36	3.04	4.62	0.823 ± 0.004	1.07	24
125.0	UJ42	EC	60.32	1.69	2.80	1.92	3.18	0.825 ± 0.010	1.07	46
125.0	UJ42	MIC-M	–	–	–	–	–	–	–	–
120.0	UJ39	OC	64.46	1.53	2.37	1.82	2.82	0.821 ± 0.002	1.00	33
120.0	UJ39	EC	–	–	–	–	–	–	–	–
111.0	UJ38	EC	65.80	1.30	1.98	1.63	2.48	0.821 ± 0.006	1.61	22
111.0	UJ38	MIC-C	–	–	–	–	–	–	–	–
99.0	UJ33	MIC-C	23.54	6.44	27.36	6.45	27.40	0.819 ± 0.004	0.71	26
99.0	UJ33	OC	–	–	–	–	–	–	–	–
90.5	JU12*	MIC-C	–	–	–	–	–	–	–	–
79.0	UJ26	OD	–	–	–	–	–	–	–	–
79.0	UJ26	MIC-D	–	–	–	–	–	–	–	–
79.0	UJ26	EC	–	–	–	–	–	–	–	–
72.0	UJ24b	EC	~~65.43~~	~~7.60~~	~~11.62~~	~~7.66~~	~~11.71~~	~~0.755 ± 0.042~~	~~99.12~~	~~31~~
72.0	UJ24b	OM	~~61.13~~	~~7.34~~	~~12.01~~	~~7.40~~	~~12.11~~	~~0.780 ± 0.004~~	~~10.52~~	~~31~~
72.0	UJ24b	MIC-M	~~98.35~~	~~17.58~~	~~17.87~~	~~17.65~~	~~17.95~~	~~0.830 ± 0.033~~	~~94.83~~	~~30~~
71.5	JUR8*	OD	65.11	3.27	5.02	3.41	5.24	0.821 ± 0.002	0.97	20
71.5	JUR8*	EC	66.45	1.22	1.84	1.58	2.38	0.813 ± 0.011	1.62	15
69.0	UJ23	EC	63.37	0.61	0.96	1.13	1.78	0.826 ± 0.005	1.30	23
69.0	UJ23	OM	66.96	5.95	8.89	6.04	9.02	0.817 ± 0.003	0.96	25
67.5	JUB7*	OC	65.52	2.06	3.14	2.29	3.50	0.822 ± 0.002	0.59	25
67.5	JUB7*	EC	67.32	1.63	2.42	1.92	2.85	0.828 ± 0.002	1.25	21
66.0	CH1*	OND	65.49	1.47	2.24	1.77	2.70	0.820 ± 0.002	1.02	27
66.0	CH1*	EC	61.90	2.14	3.46	2.33	3.76	0.816 ± 0.003	1.92	14
65.0	JUB6*	OND	58.88	2.43	4.13	2.58	4.38	0.818 ± 0.002	1.16	33

(*continued on next page*)

Table 1 (*continued*)

Strat. height (m)	Sample name	Carbonate phase	Age (Ma)[1]	2σ (Ma)[2]	2σ (%)[3]	$2\sigma_{ex}$ (Ma)[4]	$2\sigma_{ex}$ (%)[5]	$^{207}Pb/^{206}Pb \pm 2\sigma$[6]	MSWD[7]	n[8]
65.0	JUB6*	EC	64.73	0.96	1.48	1.37	2.12	0.830 ± 0.003	1.41	27
64.0	JUB5*	OND	65.42	2.60	3.97	2.78	4.25	0.818 ± 0.003	0.50	20
64.1	JUB5a*	EC	65.99	0.94	1.42	1.37	2.08	0.817 ± 0.004	0.98	15
64.1	JUB5b	EC	64.89	0.54	0.83	1.11	1.71	0.813 ± 0.006	1.19	30
64.1	JUB5c	EC	63.25	0.93	1.47	1.33	2.10	0.833 ± 0.010	4.59	42
63.0	UJ19	EC	64.85	0.57	0.88	1.12	1.73	0.819 ± 0.006	0.51	29
63.0	UJ19	OM	–	–	–	–	–	–	–	–
57.5	UJ17	EC	65.25	1.61	2.47	1.88	2.88	0.822 ± 0.006	1.15	21
57.5	UJ17	OM	–	–	–	–	–	–	–	–
56.0	JUB1*	OM	65.08	3.66	5.62	3.79	5.82	0.819 ± 0.005	1.59	29
55.8	UJ15	OC	64.81	2.22	3.43	2.40	3.70	0.819 ± 0.006	0.55	27
55.8	UJ15	EC	–	–	–	–	–	–	–	–
55.0	UJ14	OC	65.80	3.74	5.68	3.87	5.88	0.802 ± 0.003	0.49	24
55.0	UJ14	EC	–	–	–	–	–	–	–	–
55.0	UJ14	MIC-D	–	–	–	–	–	–	–	–
42.0	UJ12	OC	66.58	1.73	2.60	2.00	3.00	0.821 ± 0.002	0.98	30
42.0	UJ12	EC	–	–	–	–	–	–	–	–
42.0	UJ12	MIC-M	–	–	–	–	–	–	–	–
26.5	UJ7	OC	–	–	–	–	–	–	–	–
26.5	UJ7	MIC-M	–	–	–	–	–	–	–	–
25.7	UJ6a	MIC-C	66.48	0.70	1.05	1.22	1.84	0.815 ± 0.004	0.74	29
25.7	UJ6a	EC	–	–	–	–	–	–	–	–
25.7	UJ6a	OC	–	–	–	–	–	–	–	–
25.7	UJ6a	MIC-D	–	–	–	–	–	–	–	–
24.0	UJ6	OC	–	–	–	–	–	–	–	–
6.0	JUR1*	OC	–	–	–	–	–	–	–	–
5.5	UJ4	OC	–	–	–	–	–	–	–	–
4.0	UJ3	OC	~~94.42~~	~~64.28~~	~~68.08~~	~~64.30~~	~~68.10~~	~~0.841 ± 0.002~~	~~0.09~~	~~5~~
4.0	UJ3	MIC-C	–	–	–	–	–	–	–	–
2.0	UJ1	MIC-C	–	–	–	–	–	–	–	–

Notes

[1] *Lower intercept ages from carbonate Tera-Wasserburg Concordia plots.*

[2] *Absolute internal uncertainty (without including long-term excess of variance).*

[3] *Relative internal uncertainty: percent of internal uncertainty without including long-term excess of variance.*

[4] *Absolute uncertainty including long-term excess of variance (1.5%).*

[5] *Relative external uncertainty: percent of external uncertainty including long-term excess of variance.*

[6] *Initial $^{207}Pb/^{206}Pb$ ratio with associated absolute uncertainty derived from isochron y-axis intercept.*

[7] *Mean Squared Weighted Deviates.*

[8] *Number of LA-ICPMS spot analyses.*

carbonate type (i.e. microbialites, oncoids, ooids, early cements) and mineralogy (calcite, dolomite, mixed calcite-dolomite) together with the main results of the U-Pb isotopic analyses. Further details on U-Pb data are reported in Appendix A and Appendix B (Supplementary Material).

The 101 carbonate phases investigated include:

- Microbialites: 25 calcitic (MIC-C), 12 dolomitic (MIC-D), 6 mixed (MIC-M);
- Oncoids: 3 dolomitic (OND);
- Ooids: 23 calcitic (OC), 2 dolomitic (OD), 8 mixed (OM);
- Early cements: 22 calcites (EC).

Among the 101 analyzed phases 52 were datable, whereas 42 could not be dated (and are referred as "undateable") and 7 gave errorchrons (sensu Brooks et al., 1972). The latter represent ages with a "low chance of significance", since the regression lines display a low-probability-of-fit (dispersed data points), leading to high age uncertainty and/or MSWD (Brooks et al., 1972; Powell et al., 2020).

By considering only the datable phases, the obtained ages range from 67.32 ± 1.92 Ma to 23.54 ± 6.44 Ma ($13 < n < 46$; $2\sigma_{ex}$ down to 1.7%; $0.16 < MSWD < 2.09$ (one sample at 4.59); see Table 1, Appendix A and Appendix B).

Figs. 4 and 5 report petrographic features of the main carbonate types dated, together with the correspondent Tera Wasserburg Concordia diagrams.

5.2. Carbonate preserved depositional ages

To identify the preserved depositional ages and then to build a carbonate depositional age model along the Juramento section, we integrated the whole dataset of carbonate phases dated ($n = 52$), which consists of 19 phases from Montano et al. (2022) and 33 phases from this study (Table 1, Appendix B). Among them, 12 phases have dolomitic or mixed (calcite-dolomite) mineralogy; they were also considered to possibly infer depositional ages since dolomitization in the Yacoraite Fm. from the study area has been demonstrated to be a syn-depositional process (Gomes et al., 2020).

To identify the carbonate phases that record preserved depositional U-Pb composition, the ages of all datable phases were plotted, with associated uncertainties ($2\sigma_{ex}$), along the studied section together with the zircon depositional age model from Montano et al. (2022); Fig. 6A). Then the methodology proposed by Montano et al. (2022) was applied. This consisted in computing carbonate depositional weighted average ages (CDA_w) from carbonate phases from the same layer. The MSWD of the CDA_w was used to evaluate the consistency among the carbonate ages occurring in the same layer, knowing that if the ages do not record the same event the MSWD of the CDA_w is expected to be $>> 1$ (Horstwood et al., 2016; Montano et al., 2022). Accordingly, when the computed CDA_w has $MSWD >> 1$, the younger carbonate age is rejected, and the CDA_w recalculated until the MSWD criterion is satisfied. The application of this criterion to the CDA_w from the studied section allowed discarding 8 carbonate phases out of the 52 dated.

For layers where only one carbonate phase was dated, the CDA_w could not be computed, and single ages were plotted along the section. In this case, it was verified that single ages overlap within uncertainty the zircon depositional age model, and those not satisfying this criterion were also rejected. The application of this criterion allowed discarding 2 further carbonate phases.

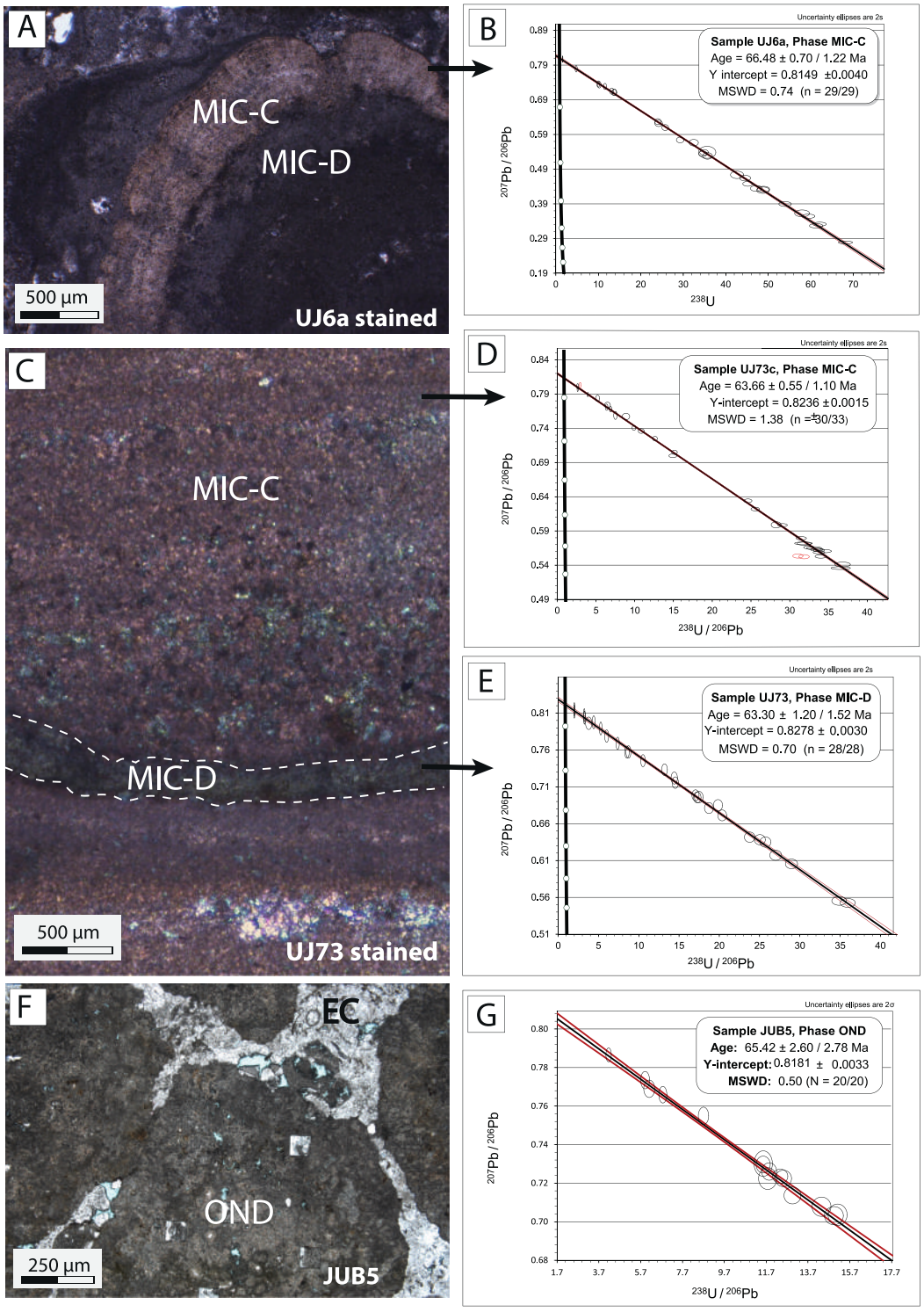

Fig. 4. Petrographic images (PPL view) of different carbonate phases and corresponding Tera Wasserburg Concordia diagrams. A. and B. Calcitic and dolomitic laminae (MIC-C and MIC-D, respectively pink stained and unstained) of fine-grained laminated stromatolite (UJ6a sample, Sequence 1). C., D., and E. Fine-grained laminated stromatolite characterized by the alternation of pink stained calcitic laminae (MIC-C) and unstained dolomitic laminae (MIC-D). UJ73 sample, Sequence 4. F. and G. Oncoidal rudstone composed of porous dolomitic spongiostromate oncoids (OND), cemented by an early equant calcite cement (EC). (For interpretation of the references to colour in this figure legend, the reader is referred to the web version of this article.)

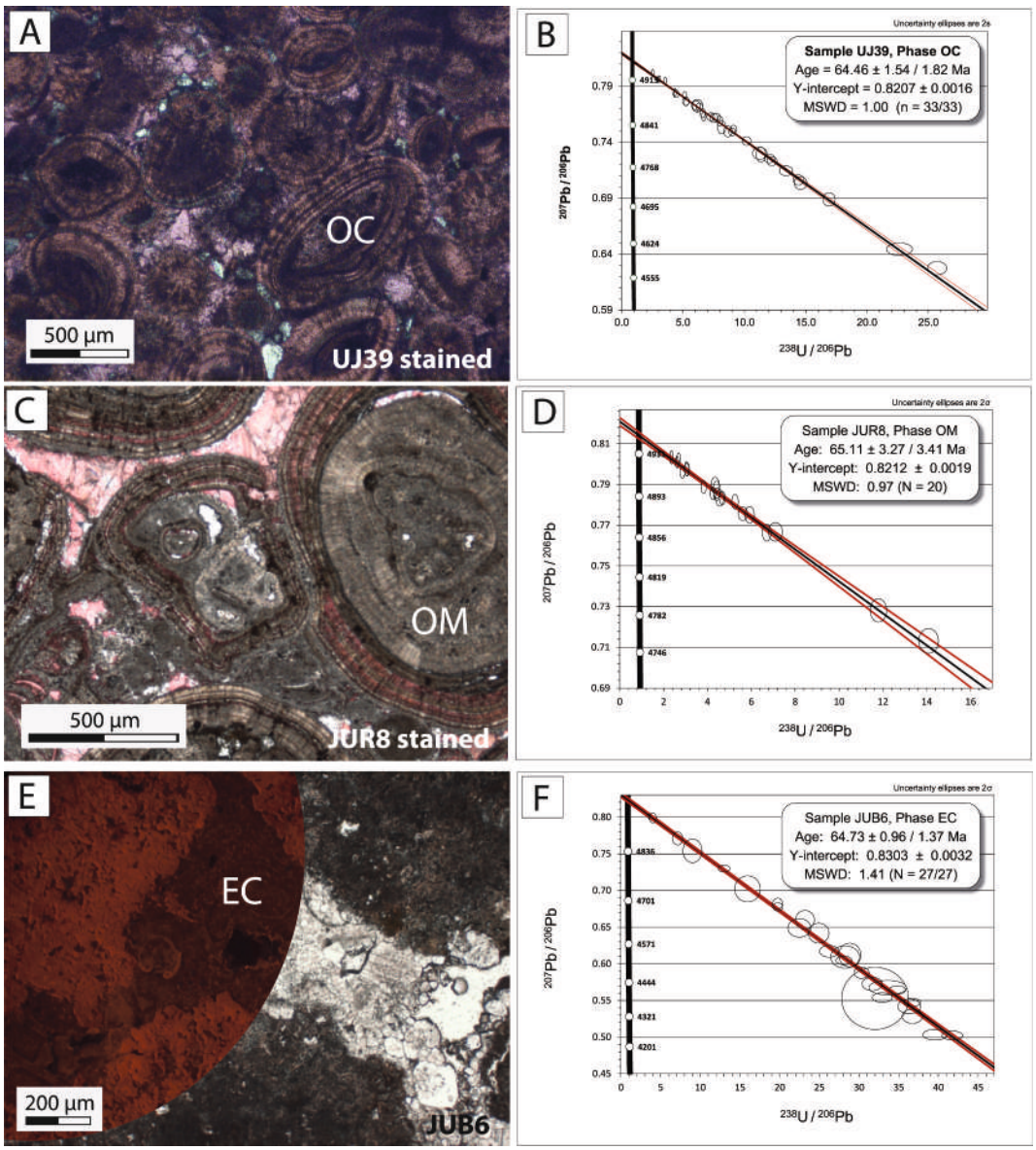

Fig. 5. Petrographic images (PPL view) of different carbonate phases and corresponding Tera Wasserburg Concordia diagrams. A. and B. Calcitic ooids (OC) in oolitic grainstone (UJ39 sample, stained). C. and D. Grapestone-ooid packstone to grainstone composed of mixed ooids (OM) displaying alternation of calcitic and dolomitic cortical laminae (JUR8 sample, stained). E. and F. Equant calcite crystals (EC) occupy the interparticle pores of an oncoidal rudstone and show a uniform dull red colour in the cathodoluminescence view (JUB6 sample). (For interpretation of the references to colour in this figure legend, the reader is referred to the web version of this article.)

The 10 discarded carbonate phases were possibly modified by post-depositional diagenesis; therefore, their ages represent events younger than deposition. It is indeed known that carbonates are susceptible to diagenetic modification that may affect the U-Pb systematics and reset the original ages (Jones et al., 1995; Kelly et al., 2003; Li et al., 2014; Roberts et al., 2020a; Montano et al., 2022; Gasparrini et al., 2023). The ages of the remaining 42 carbonate phases (i.e., all datable phases except those considered younger) were considered representative of the depositional event (i.e., preserved depositional ages) and will be used for statistics (see section "5.3 Statistical and compositional analysis").

To construct an updated carbonate depositional age model, we used the approach proposed by Montano et al. (2022) along the same section, and 9 CDA_w (Fig. 6B), that satisfy the MSWD criterion explained above, were considered. The lack of hiatuses >0.1 to 0.4 Ma along the stratigraphic section (Deschamps et al., 2020) together with the linear distribution of the carbonate ages justify building a depositional age model by linear interpolation (e.g. Watson et al., 2017). The temporal resolution achieved in the updated model is between 2.6 and 3.0% and agrees with the known precision of carbonate U-Pb dating by LA-ICPMS (down to 2.0% in Guillong et al., 2020 and down to 1.4% in Montano et al., 2021).

The updated depositional age model presented here (Fig. 6B) has a better spatial resolution than the previous one (Fig. 3C; Montano et al., 2022). This results from having filled the gaps of point age-depth estimates along the stratigraphic section. The updated model allowed constraining with higher resolution the SB ages and the duration of depositional sequences (compare Fig. 6 with Fig. 3C).

5.3. Statistical and compositional analyses

The whole dataset of carbonate U-Pb geochronology from the Juramento stratigraphic section consists of 101 carbonate phases analyzed. Among them, 41.6% (n = 42) respected the criteria to be considered preserved depositional ages (see section "5.2 Carbonate preserved

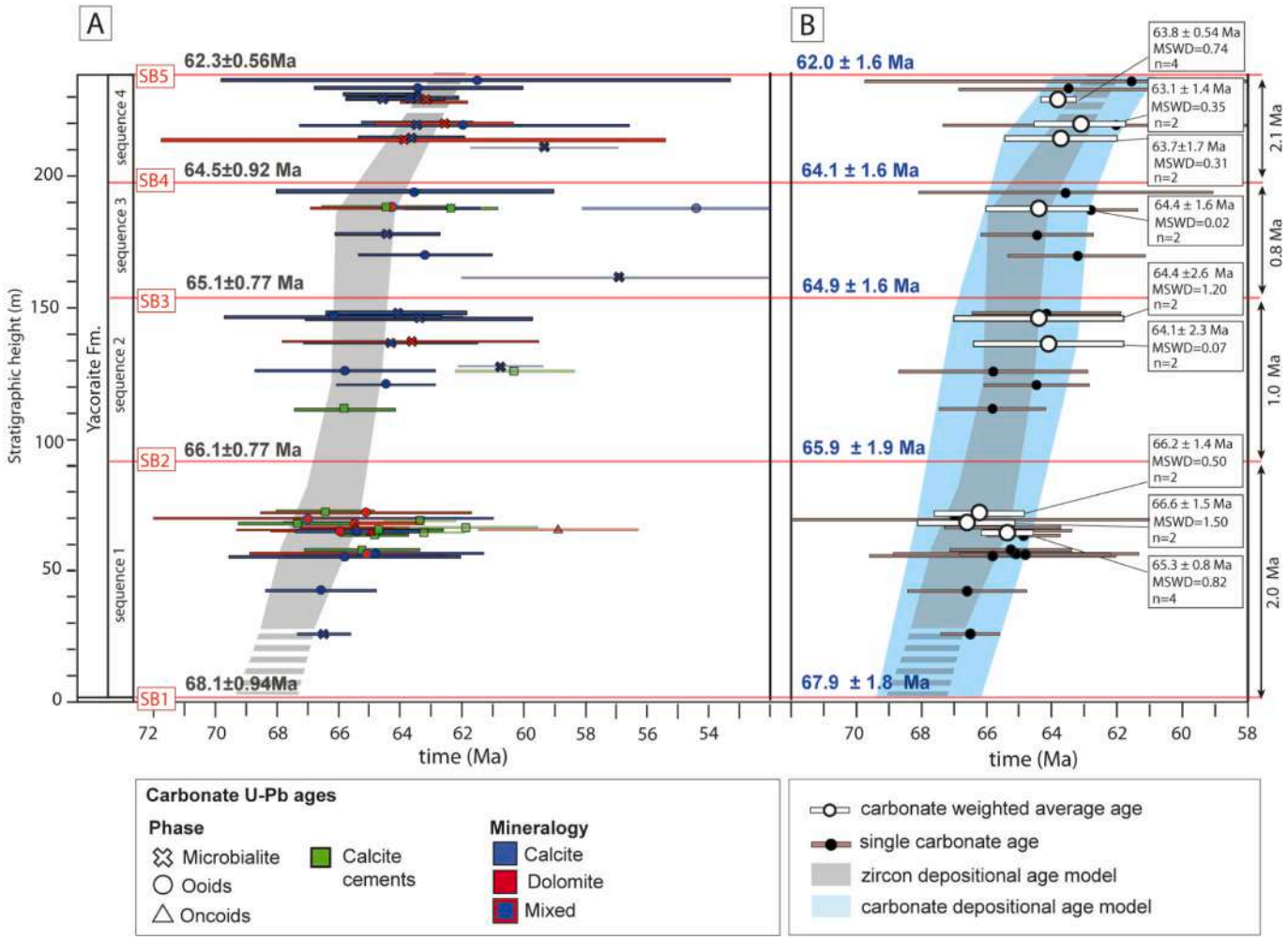

Fig. 6. Carbonate U-Pb ages and depositional age model of the Yacoraite Fm. along the Juramento section. Red lines are the sequence boundaries (SB). A. U-Pb ages and uncertainty are reported for all carbonate phases dated ($n = 52$) along the section. SB ages are from the zircon depositional age model (grey area) of Montano et al. (2022). All reported uncertainties are $2\sigma_{ex}$. B. The carbonate depositional age model constructed by linear interpolation of 9 carbonate weighted average ages (CDA_w) is represented by the light blue area and overlaps the zircon depositional age model (grey area). CDA_w were obtained from carbonate phases of the same layer that record the depositional event (see criterion in the main text). CDA_w are reported in the black frames, with the number of single carbonate ages considered (n) and the Mean Squared Weighted Deviates (MSWD) of the weighted average ages. SB ages and duration of stratigraphic sequences were inferred from the carbonate depositional age model. (For interpretation of the references to colour in this figure legend, the reader is referred to the web version of this article.)

depositional ages"), 41.6% (n = 42) could not be dated and will be here referred as "undateable", 6.9% ($n = 7$) gave errorchrons, and 9.9% ($n = 10$) resulted in ages younger than depositional age (Fig. 7A).

The U and Pb geochemistry of all the carbonate phases analyzed were also considered; in Figs. 7B-C the U and Pb contents and the $^{238}U/^{206}Pb$ and $^{207}Pb/^{206}Pb$ ratios of the single LA spot analyses are reported per carbonate class (i.e. preserved depositional, undateable, errorchron and younger). Most LA spot analyses fall in a field characterized by U contents between 0.5 and 100 ppm and Pb contents between 0.1 and 100 ppm. The $^{238}U/^{206}Pb$ and $^{207}Pb/^{206}Pb$ ratios of most LA spot analyses are below 100 and 0.85, respectively. Undateable carbonate phases (Fig. 7C) are characterized by high $^{207}Pb/^{206}Pb$ ratios ($\geq$0.8) and a limited $^{238}U/^{206}Pb$ ratio spread (mostly <6). Carbonate phases giving errorchrons are characterized by $^{207}Pb/^{206}Pb$ and $^{238}U/^{206}Pb$ ratios scattered around their linear regression and therefore hindering the construction of a statistically robust isochron (Fig. 7C). The datable carbonate phases (including both preserved depositional and younger ages) are characterized by the most variable U and Pb contents (Fig. 7B) and $^{207}Pb/^{206}Pb$ and $^{238}U/^{206}Pb$ ratios (Fig. 7C).

The distribution of age uncertainty ($2\sigma_{ex}$, %) of the carbonate phases with preserved depositional ages was investigated by statistical analysis (Fig. 8). When considering all preserved depositional ages indistinctly (42 out of 101 phases analyzed; dating success rate ~ 42%) the $2\sigma_{ex}$ uncertainties vary between 1.4 and 16.8% with a mean of 4.2%. Over 90% of the uncertainties are less than 6% ($2\sigma_{ex}$). The normal frequency distribution of uncertainties points to a mode value of 2.6% (Fig. 8A).

The frequency distribution analysis was conducted by classing the preserved depositional ages by mineralogy (calcitic, dolomitic/mixed; Fig. 8B-C) and carbonate type (microbialite/oncoids, ooids, cements; Fig. 8D-E-F).

By comparing the data classed by mineralogy (Fig. 8B-C), it comes out that the calcitic phases ($n = 70$) have a higher dating success rate (46%) compared to the phases composed partially or totally by dolomite ($n = 31$; dating success rate of 32%). The different mineralogy is also associated with various age precision: the range and mean values of the $2\sigma_{ex}$ uncertainty are 1.4–13.4% and 3.7% for calcitic phases and 2.4–16.8% and 6.0% for dolomitic/mixed phases.

By comparing the data classed by carbonate type (Fig. 8D-E-F), it can be observed that microbialites/oncoids ($n = 46$) have lower dating success rate (35%) compared to ooids ($n = 33$) and early calcite cements ($n = 22$) that reveal success rates of 49% and 46%, respectively. Concerning the age precision associated with the different carbonate types,

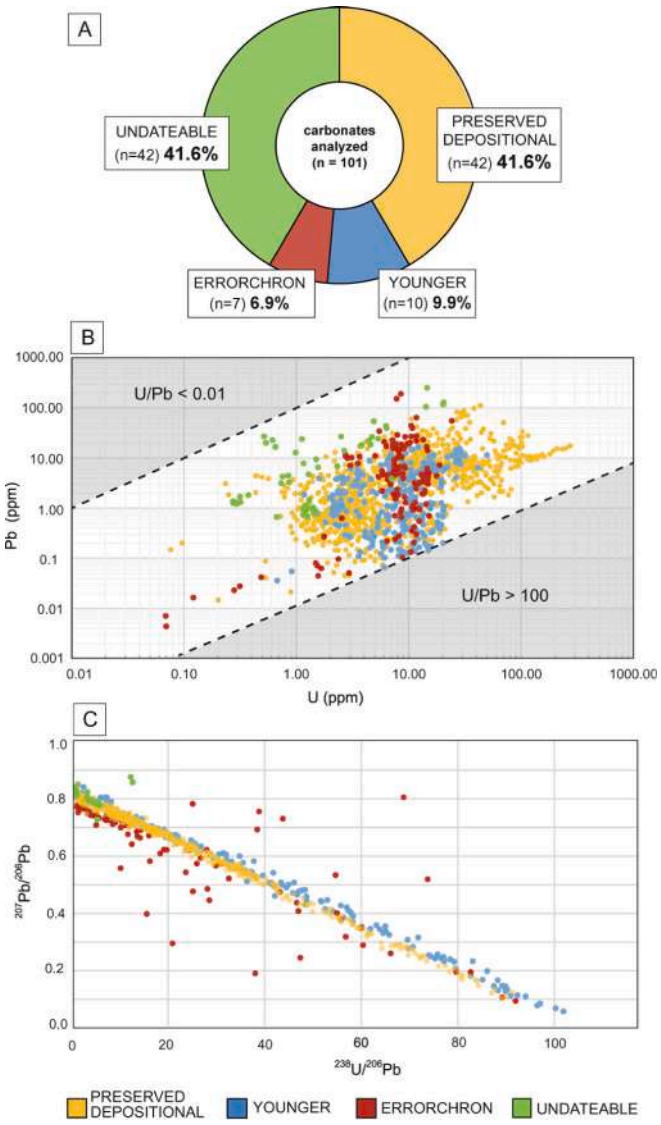

Fig. 7. A. Pie chart illustrating the general U-Pb dating success rate of the carbonates investigated. Carbonate classes were established from the whole phases analyzed (n = 101): preserved depositional (41,6%), undateable (41,6%), errorchrons (6,9%), and younger (9,9%). B. Cross-plot of Uranium (U) versus Lead (Pb) concentrations (in ppm) of the single spot LA-ICPMS analyses divided per carbonate class. The U and Pb composition of carbonates falls between the dashed lines (0.01 < U/Pb <100). C. Cross-plot of $^{238}U/^{206}Pb$ versus $^{207}Pb/^{206}Pb$ ratios of the single spot LA-ICPMS analyses divided per carbonate class.

the range and mean values of $2\sigma_{ex}$ uncertainty are 1.4–16.8% and 4.2% for microbialites/oncoids, 2.5–13.4% and 5.3% for ooids and 1.7–3.8% and 2.5% for calcite cements.

It is worth mentioning that the analytical approach chosen (section 4. Methodologies) and the obtained results could be refined by analyzing the same number of LA-spots for each carbonate phase. Based on the present results and considering that the U-Pb dating potential depends on both dating success rate and age precision (see section "6. Carbonate dating potential for chronostratigraphy"), microbialites/oncoids and ooids seem to have a lower dating potential than the calcite cements.

6. Carbonate dating potential for chronostratigraphy

Carbonate LA-ICPMS U-Pb geochronology is a promising tool for improving chronostratigraphic resolution of continental successions, though limited by the fact that not all carbonates are suitable. This depends on the dating potential of carbonates, which, in turn, depends on the probability of producing accurate and precise ages. To assess the U-Pb dating potential of carbonates, two parameters need to be evaluated: the dating success rate (i.e., the percentage of samples providing accurate ages) and the age precision.

These two parameters chiefly depend on (i) the original U-Pb carbonate composition and (ii) the sensitivity of carbonates to diagenetic modifications.

(i) The original U-Pb composition of carbonates depends on the environmental conditions and processes driving the mineral precipitation. The mechanisms of U and Pb uptake in carbonates are not fully understood and rely on the interplay of many environmental factors (Sturchio et al., 1998; Kelly et al., 2003, 2006; Cole et al., 2004; Tribovillard et al., 2006; Rasbury and Cole, 2009; Roberts et al., 2020; Rasbury et al., 2021, 2023; Miyajima et al., 2021). Assuming a closed system, statistically robust U-Pb ages should come from carbonates that initially incorporated relatively high and variable amounts of U and low and homogeneous amounts of Pb.

(ii) Carbonates are sensitive to textural and geochemical changes due to post-depositional diagenetic processes (i.e., neomorphism, recrystallization, replacement), potentially causing U-Pb age degradation or resetting. Consequently, depositional and early diagenetic carbonates may provide younger ages that record later diagenetic modifications. Carbonates originally precipitated with an unstable mineralogy (e.g., aragonite, early dolomite) are more prone to undergo these modifications (e.g., Jones et al., 1995; Kelly et al., 2003; Li et al., 2014; Roberts et al., 2020; Brigaud et al., 2021; Montano et al., 2021, 2022; Gasparrini et al., 2023). However, diagenetic processes may also affect carbonates with stable mineralogy if they are characterized by high reactive surfaces (function of grain/crystal coarseness and pore network) that may favor post-depositional interactions with fluids.

Aiming to gain insights into the dating potential of carbonates by U-Pb geochronology, samples from the same sedimentary system should be investigated to minimize the risk of introducing additional uncertainties such as different burial or diagenetic histories. The well-constrained depositional time framework for the Yacoraite Fm. from the Juramento section (Figs. 2 and 3) and the large U-Pb dataset produced from the studied section (Table 1, Fig. 6) let this section stand out as an ideal target for such purpose. The investigated carbonates proved to have good dating potential. Indeed, 42 of the 101 carbonate phases analyzed (42%) yielded accurate ages, consistent with those from zircon geochronology (Fig. 6), and record preserved depositional ages (Fig. 7). The quality of these results, both in terms of accuracy and precision ($2\sigma_{ex}$ down to 1.7%), was favored by three main factors that characterize the Yacoraite Fm. from the Juramento section (Cabra Corral Lake area, Metán sub-basin; Fig. 1B):

(i) First, the studied stratigraphic section is located close to a basin depocenter (Deschamps et al., 2020), where input of detrital clays, commonly rich in Pb, was limited. This possibly played a role since high Pb concentrations may negatively affect dating feasibility (e.g. Roberts et al., 2020; Rasbury et al., 2021);

(ii) Then, the widespread microbial activity, associated with organic matter degradation, that characterizes the deposition of the Yacoraite Fm. (Deschamps et al., 2020; Gomes et al., 2020; Villafañe et al., 2022), could have promoted the incorporation of U in the studied carbonates (e.g. Cole et al., 2004; McManus et al., 2006; Tribovillard et al., 2006);

(iii) Finally, these carbonates escaped major heating events (Romero-Sarmiento et al., 2019) and burial diagenesis was limited so that the carbonates mostly preserved pristine geochemical features

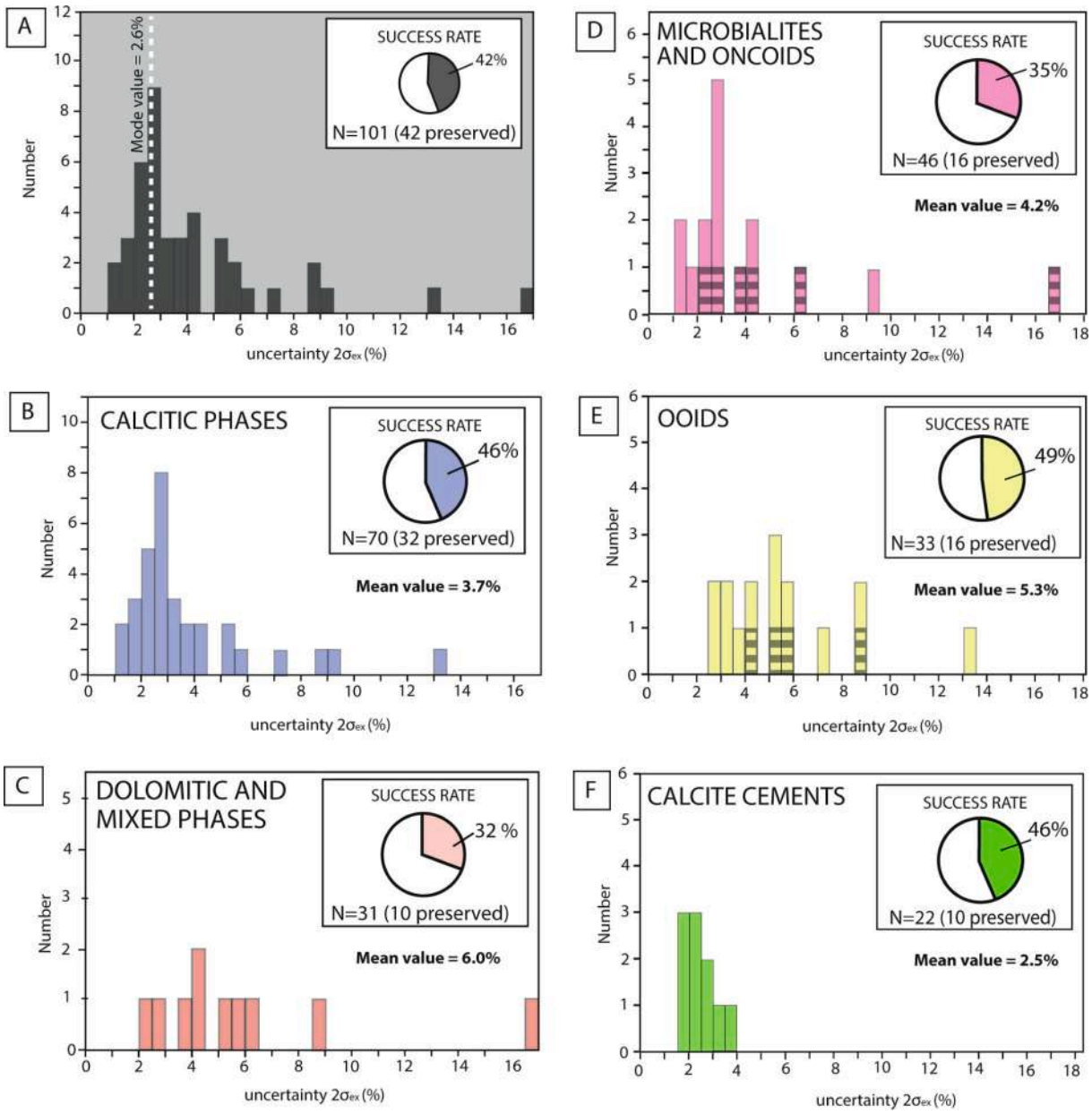

Fig. 8. Frequency distribution of carbonate age uncertainties ($2\sigma_{ex}$). A. All carbonates (n = 101) with a success rate of 42%. B. Carbonates with calcitic mineralogy ($n = 70$) with a success rate of 46%. C. Carbonates with dolomitic and mixed mineralogy ($n = 31$) with a success rate of 32%. D. Microbialite and oncoids ($n = 46$) with a success rate of 35%. The banded pattern refers to dolomitic/mixed phases. E. Ooids ($n = 33$) with a success rate of 49%. The banded pattern refers to dolomitic/mixed phases. F. Calcite cements ($n = 22$) with a success rate of 46%.

(Sial et al., 2001; Marquillas et al., 2007; Rohais et al., 2019; Gomes et al., 2020; Montano et al., 2022, 2023).

The above conditions, which possibly influenced the general availability and incorporation of U and Pb and promoted preservation of the carbonate U-Pb pristine signature after deposition, were common to the precipitation of all carbonate phases analyzed. Nevertheless, the different carbonate phases provided variable dating success rate and age precision, and therefore different dating potential (Fig. 8). This study highlighted two further factors that seem to have controlled the carbonate dating potential: the mineralogy (calcite, dolomite) and the carbonate type (microbialites, ooids, cements).

6.1. Mineralogy control

Syn-depositional carbonate phases with dolomitic or mixed (dolomite-calcite) mineralogy have a lower U-Pb dating success rate (32%; Fig. 8C) compared to those with calcitic mineralogy (46%; Fig. 8B). Also, the time resolution of the preserved depositional ages obtained from dolomitic/mixed phases is lower (mean $2\sigma_{ex}$ 6.0%; Fig. 8C), compared to the calcitic ones (mean $2\sigma_{ex}$ 3.7%; Fig. 8B). The carbonate types that occur with both mineralogies (i.e. microbialites and ooids; Fig. 4A, C, 5C) also confirm this general trend since the dolomitic/mixed phases of each carbonate type show relatively less precise ages (Fig. 8D and E). This evidence suggests that mineralogy plays a role in controlling the dating potential of the various carbonate types.

It is known that co-precipitated carbonates with different mineralogy may incorporate variable amounts of U and Pb because of the differences in crystal lattice that may promote (or not) the incorporation of these elements (e.g. Banner and Hanson, 1990; Smith et al., 1994; Reeder et al., 2000). However, literature lacks studies on statistically relevant *syn*-depositional carbonates with calcite/dolomite mineralogy that

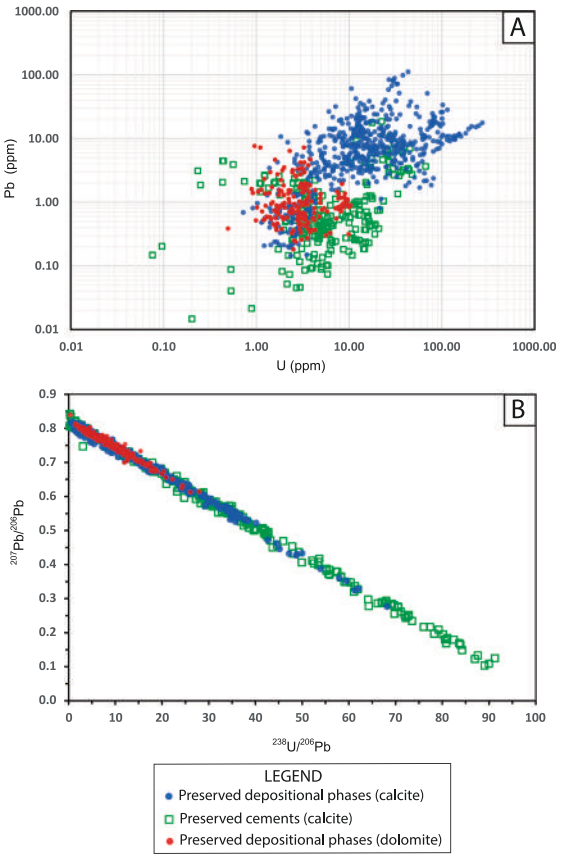

Fig. 9. Geochemical composition of the single spot LA-ICPMS analyses on carbonate phases with preserved depositional ages, classed by mineralogy. A. Cross-plot of Uranium (U) versus Lead (Pb) concentration (in ppm). B. Cross-plot of $^{238}U/^{206}Pb$ versus $^{207}Pb/^{206}Pb$ ratios.

precipitated within the same sedimentary system.

Here, we can rely on a statistically robust set of carbonates with preserved depositional ages (32 calcites and 10 dolomites/mixed) and try to correlate the age precision obtained with the U-Pb elemental and isotopic composition (Fig. 9A). In Fig. 9 we report the U versus Pb contents and the $^{238}U/^{206}Pb$ versus $^{207}Pb/^{206}Pb$ ratios of the single LA spot analyses of carbonates with preserved depositional ages, classed by mineralogy and by distinguishing depositional phases from cements. The lower age precision revealed by the dolomitic/mixed depositional phases seems to be associated with:

1) more homogeneous U-Pb contents (U 0.49–10.40 ppm, mean 3.42, and Pb 0.18–12.78 ppm, mean 2.00) compared to the calcitic phases (U 0.72–273.12 ppm, mean 25.74, and Pb 0.14–111.60 ppm, mean 9.77, for depositional phases; U 0.08–66.80 ppm, mean 9.32, and Pb 0.01–18.50 ppm, mean 1.46, for cements; Fig. 9A);

2) more homogeneous and less radiogenic $^{238}U/^{206}Pb$ and $^{207}Pb/^{206}Pb$ ratios ($^{238}U/^{206}Pb$ 0.36–28.00, mean 8.94, and $^{207}Pb/^{206}Pb$ 0.61–0.84, mean 0.75) compared to the calcitic phases ($^{238}U/^{206}Pb$ 0.63–68.18, mean 11.16 and $^{207}Pb/^{206}Pb$ 0.28–0.82, mean 0.73 for depositional phases; $^{238}U/^{206}Pb$ 0.25–91.26, mean 33.70 and $^{207}Pb/^{206}Pb$, 0.01–0.84, mean 0.56, for cements; Fig. 9B).

The overall more homogeneous composition of carbonates partially or totally made by dolomite could be related to incorporation of different amounts of U and Pb between calcite and dolomite minerals during original crystallization. An alternative scenario would call into question the early diagenetic dolomite recrystallization process. Dolomites originating early at near-surface conditions are known to be metastable and stabilize via recrystallization. This widely documented diagenetic process does not change the overall mineralogy of early-formed dolomites; it may cause chemical, crystallographic, and textural modifications (e.g. Gregg et al., 1992; Montañez and Read, 1992; Kupecz and Land, 1994; Machel, 1997; Kaczmarek and Sibley, 2014; Ryan et al., 2022), though it may also occur without inducing clear petrographic evidence (Al-Aasm and Packard, 2000; Gasparrini et al., 2023). Despite the occurrence of recrystallization, if the process stops early, U-Pb dating of dolomites may provide accurate ages consistent with stratigraphic and radiometric constraints (Elisha et al., 2021; Regnet et al., 2024), as also demonstrated by many dolomitic phases from this study that preserved depositional ages (Fig. 6A and 8C). In these cases, the main effect of recrystallization of early-formed dolomites could be the loss of U and Pb and the homogenization of the U-Pb compositions that may justify the observed degradation of the age precision (Fig. 8). This is only a hypothesis that needs further evidence from the study of U and Pb behavior during stabilization of early dolomites.

6.2. *Carbonate type control*

The carbonate types investigated consist of early lacustrine cements, microbial carbonates (microbialites s.s. and oncoids, hereafter referred microbialites) and ooids (Figs. 2, 4, and 5) and revealed different U-Pb dating potential (Fig. 8). Cements (Fig. 8F) have a high dating success rate (46%) and best age precision with mean uncertainties of 2.5% ($2\sigma_{ex}$). Ooids (Fig. 8E) have a high dating success rate (49%) and mean age uncertainties of 5.3%, while microbialites (Fig. 8D) have the lowest success rate (35%) and age mean uncertainties of 4.2%. Since the dating potential depends on both success rate and age precision, it means that cements have higher dating potential than ooids and microbialites.

Higher U concentrations are recorded (Fig. 10A) by microbialites (0.72–273.12 ppm, mean 20.60) and ooids (0.49–114.68 ppm, mean 18.75) compared to cements (0.08–66.80 ppm, mean 9.32). Thus, the high U content alone does not guarantee a high dating potential, and as already stated by previous authors (Roberts et al., 2020; Rasbury et al., 2021, 2023 and references therein), the Pb contents and U/Pb heterogeneity are two further limiting factors. In agreement with this statement (see Fig. 10A, B), cements display lower Pb contents (0.01–18.50 ppm, mean 1.36) and larger spread in the U/Pb ratios (0.25–91.26) compared to microbialites (0.14–60.71 ppm, mean 4.83; 0.63–68.17) and ooids (0.30–111.60 ppm, mean 10.80; 0.36–32.25). These compositional differences drive the precision of preserved depositional ages obtained among different carbonate types (Fig. 8). The question arising is, therefore, why carbonates from the same sedimentary system record different U and Pb compositions. We hypothesize that these compositional differences reflect the processes leading the precipitation of the three carbonate types: chemical precipitation for cements, induced or mediated by microbial activity for microbialites, and a combination of both processes for ooids. These processes in turn govern carbonate textures (i.e., grain/crystal size, porosity) and, therefore, the extension of reactive surfaces.

Cements likely precipitated very early, inorganically, with calcite mineralogy (Harris et al., 1985; Tucker and Wright, 1990) and consist of coarse equant crystals (Fig. 5E). Direct chemical precipitation from lacustrine waters, stable calcite mineralogy, and low reactive surface (due to coarse crystallinity and lack of micropores), limited diagenesis alteration of initial U-Pb compositions, promoting higher dating potential (Fig. 8F).

Microbialites form by the vital actions of benthic microbial communities, particularly cyanobacteria and algae, that induce or mediate carbonate precipitation, are enveloped by extracellular polymeric substances (EPS; Decho, 1990; Wingender et al., 1999) and may incorporate surrounding sediments via trapping and binding processes (e.g. Pentecost, 1991; Moore and Burne, 1987; Riding, 1991, 2000; Suarez-Gonzalez et al., 2019). Ooids are subspherical concretions with cortical laminae of carbonate crystals accreting around a nucleus, that commonly form in agitated supersaturated waters. Ooids were

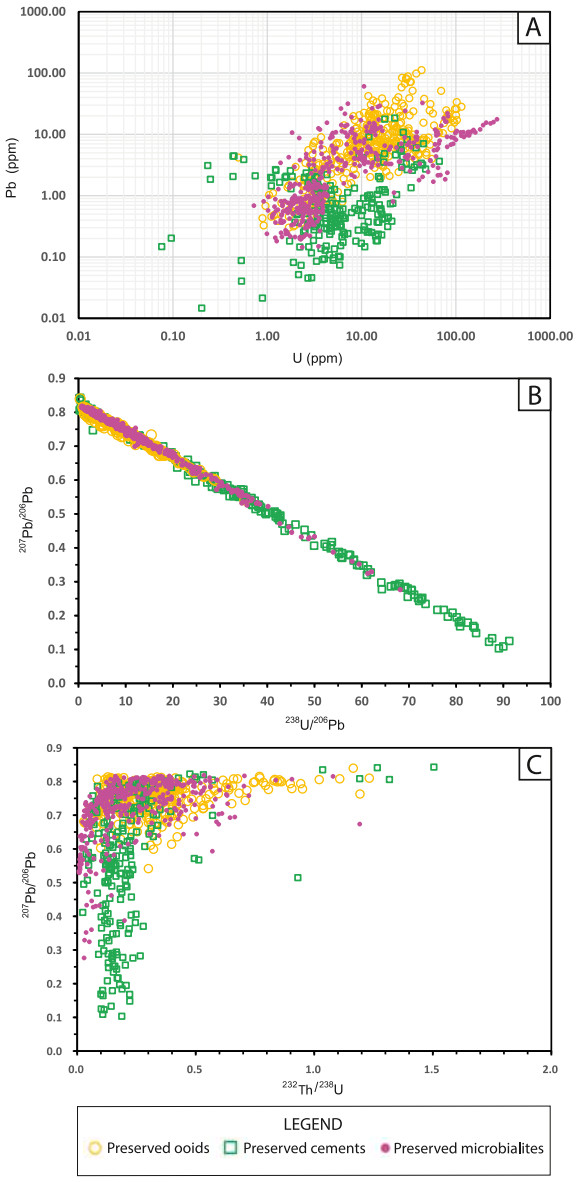

Fig. 10. Geochemical composition of the single spot LA-ICPMS analyses on carbonate phases with preserved depositional ages, classed by carbonate type. A. Cross-plot of Uranium (U) versus Lead (Pb) concentration (in ppm). B. Cross-plot of $^{238}U/^{206}Pb$ versus $^{207}Pb/^{206}Pb$ ratios. C. Cross-plot of $^{232}Th/^{238}U$ versus $^{207}Pb/^{206}Pb$ ratios.

considered abiotic grains (Davies et al., 1978; Ferguson et al., 1978; Sumner and Grotzinger, 1993) but are now believed to be partially of microbial origin (Davaud and Girardclos, 2001; Plee et al., 2008; Pacton et al., 2012; Summons et al., 2013; Diaz et al., 2015, 2017; Diaz and Eberli, 2019; Suarez-Gonzalez and Reitner, 2021), and may incorporate organic matter (Folk and Lynch, 2001; Duguid et al., 2010; O'Reilly et al., 2017; Pei et al., 2024).

Microbial activity and degradation of organic matter, occurring during the formation of both microbialites and ooids, promoted reducing conditions favorable to U uptake, since the U(IV) reduced form is more compatible with the carbonate lattice than the U(VI) form (Sturchio et al., 1998; Cole et al., 2004; McManus et al., 2006; Tribovillard et al., 2006; Rasbury and Cole, 2009; Drake et al., 2018; Roberts et al., 2020).

Microbial trapping and binding processes incorporated fine detrital material, such as clays, into these carbonates. This could explain the high common Pb contents of microbialites and ooids (Fig. 10A), provided that initial Pb partitioning from water was not the main control. This issue can be discussed by observing the Thorium (Th) contents and the relationship between $^{232}Th/^{238}U$ and $^{207}Pb/^{206}Pb$ ratios of the carbonates analyzed (Fig. 10C; Appendix A). ^{232}Th, the main naturally occurring isotope of Th, decays in the stable ^{208}Pb and is not part of the ^{238}U decay chain. Th is a lithophile element, insoluble in water, that is not commonly incorporated in the carbonate lattice; therefore, its abundance may be used as a proxy for the occurrence of detrital silicates. In pure carbonates, ^{232}Th concentration is relatively low, generally <0.5 ppm, though with a variable range (e.g., 0.1–1.0 ppm; Taylor and McLennan, 1985; Plank and Langmuir, 1998; Zhao and Zheng, 2014) which depends on age and conditions of carbonate precipitation. Elevated ^{232}Th in carbonates has been attributed to the presence of clay minerals, which are aluminosilicates, based on the covariance between Al and ^{232}Th (Singh et al., 2003).

Microbialites and ooids displayed higher $^{232}Th/^{238}U$ ratios compared to cements though they are also the richest in U (Fig. 10). A threshold of ~0.3 in the $^{232}Th/^{238}U$ ratio (Fig. 10C) seems to discriminate purely chemical cements (incorporating minimal detrital material) from microbialites and ooids (trapping more detrital clays). The clays were coeval with these carbonates because of the direct covariance between Th and common Pb contents; indeed, the datapoints with $^{232}Th/^{238}U$ above the 0.3 threshold also display $^{207}Pb/^{206}Pb$ higher than 0.65–0.70 (Fig. 10C; Appendix A). These arguments suggest that the higher Pb recorded in microbialites and ooids was mostly due to clays trapped during microbial activity and biomineralization rather than initial partitioning of higher amounts of Pb from water.

Detrital clay incorporation is likely not the sole factor lowering dating potential of microbialites and ooids; *syn-* to post-depositional diagenesis possibly also played a role. Microbialites contain growth-framework and fenestral pores and are commonly composed of micritic material with fine crystallinity and microporosity (e.g. Vanorio et al., 2009; Deville de Perière et al., 2011; Vincent et al., 2025). Oolitic packstones to grainstones are characterized by interparticle pores, and ooids themselves often develop intraparticle micropores through micritization and aragonite stabilization (e.g. Kopaska-Merkel, 1988; Sellwood and Beckett, 1991; Casteleyn et al., 2010; Hollis et al., 2017). These features cause higher reactive surface, that facilitate U-Pb mobilization during diagenesis, and that could have further lowered the dating potential of microbialites and ooids compared to cements.

In conclusion, all carbonate types formed in environments promoting incorporation of U and compositions that favored U-Pb dating (Fig. 8A). However, microbialites and ooids contain higher common Pb (that lowered age precision compared to cements) due to trapping of detrital clays, as also supported by their higher Th contents (Fig. 10C). Diagenesis would have further boosted the dating potential of cements which carry low reactive surface compared to ooids and especially microbialites.

7. Conclusions

A continuous stratigraphic section of the Maastrichtian-Danian Yacoraite Fm. from the Salta Rift was analyzed to gain insights into the general U-Pb LA-ICPMS dating potential of lacustrine carbonates for chronostratigraphy purposes. Among the 101 different syn-sedimentary carbonate phases investigated (including depositional material and early diagenetic cements) 41.6% could not be dated, 6.9% gave error-chrons, and 51.5% were dateable. These latter were further distinguished in phases preserving depositional ages ($n = 42$; 41.6%) and phases with ages younger than deposition ($n = 10$; 9.9%). Criteria to discriminate younger ages were applied and a robust carbonate depositional age model was constructed from linear interpolation of preserved depositional ages by applying a weighted average age approach. The carbonate depositional age model leads to chronostratigraphic constraints (sequence boundary ages, depositional sequence duration) that are consistent with those derived from zircon U-Pb geochronology,

demonstrating the high accuracy of the carbonate U-Pb data.

Statistical analysis of the preserved depositional ages and their relative uncertainties ($2\sigma_{ex}$) highlights that the different carbonates have variable dating potential, a function of dating success rate and age precision. The data point towards two factors that may have partially controlled the carbonate U-Pb dating potential: the mineralogy (calcite, dolomite) and the carbonate type (cements, microbialites, ooids), that in turn reflects the dominant precipitation processes (chemical, induced or mediated by microbial activity), and textures (grain/crystal size and primary pore network).

The highest dating potential is displayed by the early calcite cements precipitated via chemical processes and characterized by low reactive surface (coarse crystals, no microporosity). Conversely, ooids and microbialites have lower dating potential possibly due to 1) higher initial Pb due to incorporation of coeval detrital clays by trapping processes and 2) higher reactive surfaces (fine crystals, microporosity) promoting diagenetic modifications and consequent U-Pb age degradation or reset. Early dolomitization of the sedimentary carbonates would have also disfavored their dating potential.

This study highlights some predicting criteria of continental carbonate U-Pb dating potential for applications in chronostratigraphy. It paves the ground for further understanding and advances in this domain that could be achieved by applying the proposed analytical approach (possibly refined by analyzing the same number of LA-spots for each carbonate phase) to other well-time-framed continental carbonate successions.

CRediT authorship contribution statement

Marta Gasparrini: Conceptualization, Funding acquisition, Investigation, Project administration, Supervision, Writing – original draft, Resources, Visualization. **Damaris Montano:** Formal analysis, Investigation, Visualization. **Richard Albert:** Data curation, Formal analysis, Supervision, Writing – review & editing. **Sébastien Rohais:** Resources, Supervision, Writing – review & editing. **Axel Gerdes:** Data curation, Formal analysis, Supervision. **Andrea Ceriani:** Funding acquisition, Writing – review & editing.

Declaration of competing interest

None.

Acknowledgements

IFP Energies nouvelles is thanked for funding the PhD of Damaris Montano (2017-2021), during which most U-Pb analyses were achieved. The research was further supported by the Khalifa University of Science and Technology under the Award No. CIRA-2021-048 and by the Italian Ministry for Universities and Research (MUR) through the project "*Dipartimenti di Eccellenza 2023-27*". The authors RA and AG want to acknowledge this work as FIERCE contribution number 231. FIERCE is financially supported by the Wilhelm and Else Heraeus Foundation and by the Deutsche Forschungsgemeinschaft (DFG). Two anonymous reviewers are thanked for detailed revisions that have led to improvements in the original manuscript. Journal editors are also thanked for handling the manuscript and suggestions.

Appendix A. Supplementary data

Supplementary data to this article can be found online at https://doi.org/10.1016/j.palaeo.2026.113625.

Data availability

The authors confirm that all data necessary for supporting the scientific findings of this paper have been provided.

References

Aguirre Palafox, L.E., Möller, A., McLean, N.M., Ludvigson, G.A., Colombi, C.E., Montañez, I.P., 2024. U–Pb geochronology of paleosol carbonate cements by LA-ICPMS: a proof of concept and strategy for dating the terrestrial record. Geochem. Geophys. Geosyst. 25, e2024GC011488. https://doi.org/10.1029/2024GC011488. Geochem. Geophys. Geosyst.

Al-Aasm, I.S., Packard, J.J., 2000. Stabilization of early-formed dolomite: a tale of divergence from two Mississippian dolomites. Sediment. Geol. 131, 97–108. https://doi.org/10.1016/S0037-0738(99)00132-3.

Banner, L., Hanson, G.N., 1990. Calculation of simultaneous isotopic and trace element variations during water-rock interaction with applications to carbonate diagenesis. Geochim. Cosmochim. Acta 54 (11), 3123–3137. https://doi.org/10.1016/0016-7037(90)90128-8.

Bilau, A., Bienveignant, D., Rolland, Y., Boschetti, L., Dumont, T., 2023. The tertiary structuration of the Western Subalpine foreland deciphered by calcite-filled faults and veins. Earth Sci. Rev. 236, 104270. https://doi.org/10.1016/j.earscirev.2022.104270.

Brigaud, B., Andrieu, S., Blaise, T., Haurine, F., Barbarand, J., 2021. Calcite uranium–lead geochronology applied to hardground lithification and sequence boundary dating. Sedimentology 68, 168–195. https://doi.org/10.1111/sed.12795.

Brooks, C., Hart, S.R., Wendt, I., 1972. Realistic use of two-error regression treatments as applied to rubidium-strontium data. Rev. Geophys. 10 (2), 551–577. https://doi.org/10.1029/RG010i002p00551.

Carrera, N., Muñoz, J.A., Sàbat, F., Roca, E., Mon, R., 2006. The role of inversion tectonics in the structure of the Cordillera oriental (Argentinean Andes). J. Struct. Geol. 28, 1921–1932. https://doi.org/10.1016/j.jsg.2006.07.006.

Carrera, N., Muñoz, J.A., Roca, E., 2009. 3D reconstruction of geological surfaces by the equivalent dip-domain method: an example from field data of the Cerro Bayo Anticline (Cordillera oriental, NW argentine Andes). J. Struct. Geol. 31, 1573–1585. https://doi.org/10.1016/j.jsg.2009.08.006.

Casteleyn, L., Robion, P., Collin, P.-Y., Menéndez, B., David, C., Desaubliaux, G., Fernandes, N., Dreux, R., Badiner, G., Brosse, E., Rigollet, C., 2010. Interrelations of the petrophysical, sedimentological and microstructural properties of the Oolithe Blanche Formation (Bathonian, saline aquifer of the Paris Basin). Sediment. Geol. 230 (3–4), 123–138. https://doi.org/10.1016/j.sedgeo.2010.07.003.

Cole, J.M., Rasbury, E.T., Montañez, I.P., Pedone, V.A., Lanzirotti, A., Hanson, G.N., 2004. Petrographic and trace element analysis of uranium-rich tufa calcite, middle Miocene Barstow Formation, California, USA: Uranium-rich tufa deposits, California. Sedimentology 51, 433–453. https://doi.org/10.1111/j.1365-3091.2004.00631.x.

Cruset, D., Vergés, J., Albert, R., Gerdes, A., Benedicto, A., Cantarero, I., Travé, A., 2020. Quantifying deformation processes in the SE Pyrenees using U-Pb dating of fracture-filling calcites. J. Geol. Soc. Lond. https://doi.org/10.1144/jgs2020-014.

Davaud, E., Girardclos, S., 2001. Recent freshwater ooids and oncoids from western Lake Geneva (Switzerland): indications of a common organically mediated origin. J. Sediment. Res. 71, 423–429. https://doi.org/10.1306/2DC40950-0E47-11D7-8643000102C1865D.

Davies, P.J., Bubela, B., Ferguson, J., 1978. The formation of ooids. Sedimentology 25, 703–730. https://doi.org/10.1111/j.1365-3091.1978.tb00326.x.

Decho, A.W., 1990. Microbial exopolymer secretions in ocean environments: their role(s) in food webs and marine processes. Oceanogr. Mar. Biol. Annu. Rev. 28, 73–153.

Deschamps, R., Kohler, E., Gasparrini, M., Durand, O., Euzen, T., Nader, F.H., 2012. Impact of mineralogy and diagenesis on reservoir quality of the lower cretaceous Upper Mannville Formation (Alberta, Canada). Oil Gas Sci. Technol. Revue d'IFP Energies nouvelles 67 (1), 31–58. https://doi.org/10.2516/ogst/2011153.

Deschamps, R., Rohais, S., Hamon, Y., Gasparrini, M., 2020. Dynamic of a lacustrine sedimentary system during late rifting at the Cretaceous–Palaeocene transition: Example of the Yacoraite Formation, Salta Basin, Argentina. Depositional Rec. 6, 490–523. https://doi.org/10.1002/dep2.116.

Deville de Perière, M., Durlet, C., Vennin, E., Lambert, L., Bourillot, R., Caline, B., Poli, E., 2011. Morphometry of micrite particles in cretaceous microporous limestones of the Middle East: influence on reservoir properties. Mar. Pet. Geol. 28 (9), 1727–1750. https://doi.org/10.1016/j.marpetgeo.2011.05.002.

Diaz, M.R., Eberli, G.P., 2019. Decoding the mechanism of formation in marine ooids: a review. Earth-Sci. Rev. 190, 536–556. https://doi.org/10.1016/j.earscirev.2018.12.016.

Diaz, M.R., Swart, P.K., Eberli, G.P., Oehlert, A.M., Devlin, Q., Saeid, A., Altabet, M.A., 2015. Geochemical evidence of microbial activity within ooids. Sedimentology 62, 2090–2112. https://doi.org/10.1111/sed.12218.

Diaz, M.R., Eberli, G.P., Blackwelder, P., Phillips, B., Swart, P.K., 2017. Microbially mediated organomineralization in the formation of ooids. Geology 45, 771–774. https://doi.org/10.1130/G39159.1.

Dickson, J.A.D., 1966. Carbonate identification and genesis as revealed by staining. J. Sediment. Petrol. 36 (2), 491–505. https://doi.org/10.1306/74D714F6-2B21-11D7-8648000102C1865D.

Drake, H., Mathurin, F.A., Zack, T., Schäfer, T., Roberts, N.M.W., Whitehouse, M., Karlsson, A., Broman, C., Åström, M.E., 2018. Incorporation of metals into calcite in a deep anoxic granite aquifer. Environ. Sci. Technol. 52 (2), 493–502. https://doi.org/10.1021/acs.est.7b05258.

Drost, K., Chew, D., Petrus, J.A., Scholze, F., Woodhead, J.D., Schneider, J.W., Harper, D.A.T., 2018. An image mapping approach to U-Pb LA-ICP-MS carbonate dating and applications to direct dating of carbonate sedimentation. Geochem. Geophys. Geosyst. 19, 4631–4648. https://doi.org/10.1029/2018GC007850.

Duguid, S.M.A., Kyser, T.K., James, N.P., Rankey, E.C., 2010. Microbes and ooids. J. Sediment. Res. 80, 236–251. https://doi.org/10.2110/jsr.2010.027.

Dunham, R.J., 1962. Classification of carbonate rocks according to depositional texture. In: Ham, W.E. (Ed.), Classification of Carbonate Rocks. AAPG Memoir, 1, pp. 108–121.
Durieux, C.G., Brown, A.C., 2007. Geological context, mineralization, and timing of the Juramento sediment-hosted stratiform copper-silver deposit, Salta district, Northwestern Argentina. Mineral. Deposita 42, 879–899. https://doi.org/10.1007/s00126-007-0138-2.
Elisha, B., Nuriel, P., Kylander-Clark, A., Weinberger, R., 2021. Towards in-situ U–Pb dating of dolomites. Geochronology 3, 337–349. https://doi.org/10.5194/gchron-2020-19.
Ferguson, J., Bubela, B., Davies, P.J., 1978. Synthesis and possible mechanism of formation of radial carbonate ooids. Chem. Geol. 22, 285–308. https://doi.org/10.1016/0009-2541(78)90037-2.
Folk, R.L., Lynch, F.L., 2001. Organic matter, putative nannobacteria and the formation of ooids and hardgrounds. Sedimentology 48 (2), 215–229. https://doi.org/10.1046/j.1365-3091.2001.00354.x.
Frisch, K., Voigt, S., Verestek, V., Appel, E., Albert, R., Gerdes, A., Arndt, I., Raddatz, J., Voigt, T., Weber, Y., Batenburg, S.J., 2019. Long-period astronomical forcing of westerlies' strength in Central Asia during Miocene climate cooling. Paleoceanogr. Paleoclimatol. 34 (11), 1784–1806. https://doi.org/10.1029/2019PA003642.
Gasparrini, M., Morad, D., Mangenot, X., Bonifacie, M., Morad, S., Nader, F.H., Gerdes, A., 2023. Dolomite recrystallization revealed by Δ_{47}/U-Pb thermochronometry in the Upper Jurassic Arab Formation, United Arab Emirates. Geology 51 (5), 471–475. https://doi.org/10.1130/G50960.1.
Gasparrini, M., Mangenot, X., Bonifacie, M., Deschamps, P., Ceriani, A., 2025. Cooling and exhumation history of the Paris Basin southeastern margin revealed by Δ_{47}/U-Pb carbonate thermochronology. Terra Nova 37 (6), 421–430. https://doi.org/10.1111/ter.70004.
Gerdes, A., Zeh, A., 2006. Combined U–Pb and Hf isotope LA-(MC-) ICP-MS analyses of detrital zircons: comparison with SHRIMP and new constraints for the provenance and age of an Armorican metasediment in Central Germany. Earth Planet. Sci. Lett. 249 (1–2), 47–61. https://doi.org/10.1016/j.epsl.2006.06.039.
Gerdes, A., Zeh, A., 2009. Zircon formation versus zircon alteration-new insights from combined V-Ph and Lu-Hf in situ LA-ICP-MS analyses, and consequences for the interpretation of Archean zircon from the Central Zone of the Limpopo Belt. Chem. Geol. 261 (3–4), 230–243. https://doi.org/10.1016/j.chemgeo.2008.03.005.
Gomes, J.P.B., Bunevich, R.B., Tonietto, S.N., Alves, D.B., Santos, J.F., Whitaker, F.F., 2020. Climatic signals in lacustrine deposits of the Upper Yacoraite Formation, Western Argentina: evidence from clay minerals, analcime, dolomite and fibrous calcite. Sedimentology 67, 2282–2309 doi:10.1-111/sed.12700.
Guillong, M., Wotzlaw, J.F., Looser, N., Laurent, O., 2020. Evaluating the reliability of U–Pb laser ablation inductively coupled plasma mass spectrometry (LA-ICP-MS) carbonate geochronology: matrix issues and a potential calcite validation reference material. Geochronology 2, 155–167. https://doi.org/10.5194/gchron-2-155-2020.
Gregg, J.M., Howard, S.A., Mazzullo, S.J., 1992. Early diagenetic recrystallization of Holocene (<3000 years old) peritidal dolomites, Ambergris Cay, Belize. Sedimentology 39, 143–159. https://doi.org/10.1111/j.1365-3091.1992.tb01027.x.
Guillong, M., Samankassou, E., Müller, I.A., Szymanowski, D., Looser, N., Tavazzani, L., Merino-Tomé, Ó., Bahamonde, J.R., Buret, Y., Ovtcharova, M., 2024. Technical note: RA138 calcite U–Pb LA-ICP-MS primary reference material. Geochronology 6, 465–474. https://doi.org/10.5194/gchron-6-465-2024.
Harris, P.M., Kendall, C.G.St.C., Lerche, I., 1985. Carbonate Cementation—A Brief Review. In: Schneidermann, Nahum, Harris, Paul M. (Eds.), Carbonate Cements: Based on a Symposium Sponsored by the Society of Economic Paleontologists and Mineralogists. https://doi.org/10.2110/pec.85.36.0079.
Hoareau, G., Claverie, F., Pecheyran, C., Paroissin, C., Grignard, P., Motte, G., Chailan, O., Girard, J., 2021. Direct U–Pb dating of carbonates from micron-scale femtosecond laser ablation inductively coupled plasma mass spectrometry images using robust regression. Geochronology 3, 67–87. https://doi.org/10.5194/gchron-3-67-2021.
Hollis, C., Lawrence, L.A., Deville de Perière, M., Al Darmaki, F., 2017. Controls on porosity preservation within a Jurassic oolitic reservoir complex, UAE. Mar. Pet. Geol. 88, 888–906. https://doi.org/10.1016/j.marpetgeo.2017.09.015.
Hopley, P.J., Reade, H., Parrish, R., De Kock, M., Adams, J.W., 2019. Speleothem evidence for C3 dominated vegetation during the late Miocene (Messinian) of South Africa. Rev. Palaeobot. Palynol. 264, 75–89. https://doi.org/10.1016/j.revpalbo.2019.02.006.
Horstwood, M.S.A., Košler, J., Gehrels, G., Jackson, S.E., McLean, N.M., Paton, C., Pearson, N.J., Sircombe, K., Sylvester, P., Vermeesch, P., Bowring, J.F., Condon, D.J., Schoene, B., 2016. Community-derived standards for LA-ICP-MS U-(Th-)Pb geochronology – uncertainty propagation, age interpretation and data reporting. Geostand. Geoanal. Res. 40 (3), 311–332. https://doi.org/10.1111/j.1751-908X.2016.00379.x.
Jones, C.E., Halliday, A.N., Lohmann, K.C., 1995. The impact of diagenesis on high-precision UPb dating of ancient carbonates: an example from the late Permian of New Mexico. Earth Planet. Sc. Lett. 134 (3–4), 409–423. https://doi.org/10.1016/0012-821X(95)00128-Y.
Kaczmarek, S.E., Sibley, D.F., 2014. Direct physical evidence of dolomite recrystallization. Sedimentology 61, 1862–1882. https://doi.org/10.1111/sed.12119.
Kelly, S.D., Newville, M., Cheng, L.R., Kemner, K.M., Sutton, S.R., Fenter, P., Sturchio, N. C., Spötl, C., 2003. Uranyl incorporation in natural Calcite. Environ. Sci. Technol. 37 (7). https://doi.org/10.1021/es025962f.
Kelly, S.D., Rasbury, E.T., Chattopadhyay, S., Kropf, A.J., Kemner, K.M., 2006. Evidence of a stable uranyl site in ancient organic-rich calcite. Environ. Sci. Technol. 40, 2262–2268. https://doi.org/10.1021/es051970v.
Kopaska-Merkel, D.C., 1988. Microporosity and production potential in ooids: Mesozoic and paleozoic of Texas. Carbonates Evaporites 2, 125–131. https://doi.org/10.1007/BF03174312.
Kupecz, J.A., Land, L.S., 1994. Progressive recrystallization and stabilization of early-stage dolomite: lower ordovician ellenburger group, West Texas. In: Purser, B., Tucker, M., Zenger, D. (Eds.), Dolomites: a volume in honour of Dolomieu. IAS Special Publication, pp. 255–279. https://doi.org/10.1002/9781444304077.ch15.
Kurumada, Y., Aoki, S., Aoki, K., Kato, D., Saneyoshi, M., Tsogtbaatar, K., Windley, B.F., Ishigaki, S., 2020. Calcite U–Pb age of the Cretaceous vertebrate-bearing Bayn Shire Formation in the Eastern Gobi Desert of Mongolia: Usefulness of caliche for age determination. Terra Nova 32 (4), 246–252. https://doi.org/10.1111/ter.12456.
Lachniet, M.S., Bernal, J.P., Asmerom, Y., Polyak, V., 2012. Uranium loss and aragonite–calcite age discordance in a calcitized aragonite stalagmite. Quat. Geochronol. 14, 26–37. https://doi.org/10.1016/j.quageo.2012.08.003.
Li, Q., Parrish, R.R., Horstwood, M.S.A., McArthur, J.M., 2014. U–Pb dating of cements in Mesozoic ammonites. Chem. Geol. 376, 76–83. https://doi.org/10.1016/j.chemgeo.2014.03.020.
Liivamägi, S., Środoń, J., Bojanowski, M.J., Gerdes, A., Stanek, J.J., Williams, L., Szczerba, M., 2018. Paleosols on the Ediacaran basalts of the east European Craton: a unique record of paleoweathering with minimum diagenetic overprint. Precambrian Res. 316, 66–82. https://doi.org/10.1016/j.precamres.2018.07.020.
Looser, N., Madritsch, H., Guillong, M., Wohlwend, S., Bernasconi, S.M., 2021. Absolute age and temperature constraints on deformation along the Basal Décollement of the Jura Fold-and-Thrust belt from carbonate U-Pb dating and clumped isotopes. Tectonics 40 (3), e2020TC006439. https://doi.org/10.1029/2020TC006439.
Ludwig, K.R., 2012. User's Manual for Isoplot Version 3.75–4.15: a Geochronological Toolkit for Microsoft Excel. Berkeley Geochronological Center (Special Publication, 5).
Machel, H.G., 1997. Recrystallization *versus* neomorphism, and the concept of significant recrystallization in dolomite research. Sediment. Geol. 113, 161–168. https://doi.org/10.1016/S0037-0738(97)00078-X.
Madritsch, H., Looser, N., Schneeberger, R., Guillong, M., Malz, A., 2024. Reconstructing the evolution of foreland fold-and-thrust belts using U-Pb calcite dating: an integrated case-study from the Easternmost Jura Mountains (Switzerland). Tectonics 43 (5), e2023TC008181. https://doi.org/10.1029/2023TC008181.
Mangenot, X., Gasparrini, M., Gerdes, A., Bonifacie, M., Rouchon, V., 2018. An emerging thermochronometer for carbonate-bearing rocks: Δ_{47} /(U-Pb). Geology 46, 1067–1070. https://doi.org/10.1130/G45196.1.
Marquillas, R.A., 1985. Estratigrafıa, sedimentologıa y paleoambientes de la Formacion Yacoraite (Cretacico Superior) en el tramo austral de la cuenca, norte argentino. PhD Thesis, Universidad Nacional de Salta, 1–139.
Marquillas, R.A., Sabino, I., Sial, N.A., Del Papa, C., Ferreira, V., Matthews, S., 2007. Carbon and oxygen isotopes of Maastrichtian-Danian shallow marine carbonates: Yacoraite Formation, northwestern Argentina. J. S. Am. Earth Sci. 23 (4), 304–320. https://doi.org/10.1016/j.jsames.2007.02.009.
McManus, J., Berelson, W.M., Severmann, S., Poulson, R.L., Hammond, D.E., Klinkhammer, G.P., Holm, C., 2006. Molybdenum and uranium geochemistry in continental margin sediments: paleoproxy potential. Geochim. Cosmochim. Acta 70, 4643–4662. https://doi.org/10.1016/j.gca.2006.06.1564.
Meinhold, G., Roberts, N., Arslan, A., Jensen, S., Ebbestad, J., Högström, A., Taylor, W., 2020. U–Pb dating of calcite in ancient carbonates for age estimates of syn- to post-depositional processes: a case study from the upper Ediacaran strata of Finnmark. Arctic Norway Geol. Mag. 157, 1367–1372. https://doi.org/10.1017/S0016756820000564.
Miyajima, Y., Saito, A., Kagi, H., Yokoyama, T., Takahashi, Y., Hirata, T., 2021. Incorporation of U, Pb and rare Earth elements in Calcite through crystallisation from amorphous calcium carbonate: simple preparation of reference materials for microanalysis. Geostand. Geoanal. Res. 45 (1), 189–205. https://doi.org/10.1111/ggr.12367.
Monchal, V., Rateau, R., Drost, K., Gagnaison, C., Mennecart, B., Toullec, R., Torremans, K., Chew, D., 2025. U–Pb dating on calcite paleosol nodules: first absolute age constraints on the Miocene continental succession of the Paris Basin. Geochronology 7 (2), 139–156. https://doi.org/10.5194/gchron-7-139-2025.
Montañez, I.P., Read, J.F., 1992. Fluid-rock interaction history during stabilization of early dolomites, Upper Knox Group (Lower Ordovician), US Appalachians. J. Sediment. Petrol. 62, 753–778. https://doi.org/10.1306/D42679D3-2B26-11D7-8648000102C1865D.
Montano, D., Gasparrini, M., Gerdes, A., Albert, R., Della Porta, G., 2021. In-situ U-Pb dating of Ries Crater lacustrine carbonates (Miocene, South-West Germany): implications for continental carbonate chronostratigraphy. Earth Planet. Sc. Lett. 568 (1), 117011. https://doi.org/10.1016/j.epsl.2021.117011.
Montano, D., Gasparrini, M., Rohais, S., Albert, R., Gerdes, A., 2022. Depositional age models in lacustrine systems from zircon and carbonate U-Pb geochronology. Sedimentology 69, 2507–2534. https://doi.org/10.1111/sed.13000.
Montano, D., Gasparrini, M., Rohais, S., De Luca, R., 2023. A lacustrine record for the Cretaceous-Paleogene boundary - Yacoraite Fm. (North-West Argentina). Geosciences 13 (8), 227. https://doi.org/10.3390/geosciences13080227.
Moore, L.S., Burne, R.V., 1987. Microbialites: organosedimentary deposits of benthic microbial communities. Palaios 2 (3), 241–254. https://doi.org/10.2307/3514674.
Mottram, C.M., Kellett, D.A., Barresi, T., Zwingmann, H., Friend, M., Todd, A., Percival, J.B., 2020. Syncing fault rock clocks: direct comparison of U-Pb carbonate and K-Ar illite fault dating methods. Geology 48 (12), 1179–1183. https://doi.org/10.1130/G47778.1.
Mutti, M., Vallati, M., Tomás, S., Galli, C., Bahniuk Rumbelsperger, A.M., Maerz, S., Coira, B., 2023. Constraining depositional evolution and reservoir compartmentalization in a mixed carbonate-siliciclastic lacustrine system: the

Yacoraite formation, Salta Group, NW Argentina. Mar. Pet. Geol. 149, 106049. https://doi.org/10.1016/j.marpetgeo.2022.106049.
Nicholson, S.L., Pike, A.W., Hosfield, R., Roberts, N.M.W., Sahy, D., Woodhead, J., Cheng, H., Edwards, R.L., Affolter, S., Leuenberger, M., Burns, S.J., 2020. Pluvial periods in Southern Arabia over the last 1.1 million-years. Quat. Sci. Rev. 229, 106112. https://doi.org/10.1016/j.quascirev.2019.106112.
Ogg, J., Ogg, G., Gradstein, F.M.A., 2016. A Concise Geologic Time Scale. Elsevier, Amsterdam, p. 240. https://doi.org/10.1016/C2009-0-64442-1.
O'Reilly, S.S., Mariotti, G., Winter, A.R., Newman, S.A., Matys, E.D., McDermott, F., Pruss, S.B., Bosak, T., Summons, R.E., Klepac-Ceraj, V., 2017. Molecular biosignatures reveal common benthic microbial sources of organic matter in ooids and grapestones from Pigeon Cay, The Bahamas. Geobiology 15, 112–130. https://doi.org/10.1111/gbi.12196.
Pacton, M., Ariztegui, D., Wacey, D., Kilburn, M.R., Rollion-Bard, C., Farah, R., Vasconcelos, C., 2012. Going nano: a new step toward understanding the processes governing freshwater ooid formation. Geology 40, 547–550. https://doi.org/10.1130/G32846.1.
Pan, L., Shen, A., Zhao, J., Hu, A., Hao, Y., Liang, F., Feng, Y., Wang, X., Jiang, L., 2021. LA-ICP-MS U-Pb geochronology and clumped isotope constraints on the formation and evolution of an ancient dolomite reservoir: the Middle Permian of Northwest Sichuan Basin (SW China). Sediment. Geol. 407, 105728. https://doi.org/10.1016/j.sedgeo.2020.105728.
Parrish, J.T., Rasbury, E.T., Chan, A., Hasiotis, S.T., 2019. Earliest Jurassic U-Pb ages from carbonate deposits in the Navajo Sandstone, southeastern Utah, USA. Geology 47 (11), 1015–1019. https://doi.org/10.1130/G46338.1.
Pei, Y., Suarez-Gonzalez, P., Duda, J.-P., Reitner, J., 2024. Organic matter influence on ooid formation: New insights into classic examples (Great Salt Lake, USA; Triassic Germanic Basin, Germany). Sedimentology 71, 1419–1435. https://doi.org/10.1111/sed.13179.
Pentecost, A., 1991. Calcification processes in algae and cyanobacteria. In: Riding, R. (Ed.), Calcareous Algae and Stromatolites. Springer-Verlag, Berlin, pp. 3–20.
Plank, T., Langmuir, C.H., 1998. The chemical composition of subducting sediment and its consequences for the crust and mantle. Chem. Geol. 145 (3–4), 325–394. https://doi.org/10.1016/S0009-2541(97)00150-2.
Plee, K., Ariztegui, D., Martini, R., Davaud, E., 2008. Unravelling the microbial role in ooid formation – results of an in situ experiment in modern freshwater Lake Geneva in Switzerland. Geobiology 6, 341–350. https://doi.org/10.1111/j.1472-4669.2007.00140.x.
Powell, R., Green, E.C.R., Marillo Sialer, E., Woodhead, J., 2020. Robust isochron calculation. Geochronology 2, 325–342. https://doi.org/10.5194/gchron-2-325-2020.
Rasbury, E.T., Cole, J.M., 2009. Directly dating geologic events: U-Pb dating of carbonates. Rev. Geophys. 47 (3), RG3001. https://doi.org/10.1029/2007RG000246.
Rasbury, E.T., Present, T.M., Northrup, P., Tappero, R.V., Lanzirotti, A., Cole, J.M., Wooton, K.M., Hatton, K., 2021. Tools for uranium characterization in carbonate samples: case studies of natural U-Pb geochronology reference materials. Geochronology 3, 103–122. https://doi.org/10.5194/gchron-3-103-2021.
Rasbury, E.T., Piccione, G., Holt, W., Ward, W.B., 2023. Potential for constraining sequence stratigraphy and cycle stratigraphy with U-Pb dating of carbonates. Earth Sci. Rev. 243, 104495. https://doi.org/10.1016/j.earscirev.2023.104495.
Reeder, R.J., Nugent, M., Lamble, G.M., Tait, C.D., Morris, D.E., 2000. Uranyl Incorporation into Calcite and Aragonite: XAFS and Luminescence Studies. Environ. Sci. Technol. 34, 638–644. https://doi.org/10.1021/es990981j.
Regnet, J.-B., Bailly, C., Bourquin, S., Robion, P., Poujol, M., Sengelen, X., Serrano, O., Ledésert, B., 2024. Paleosol-induced early dolomitization with U-Pb age constraints and its implications for fluid pathways in ancient sandstone aquifers. Sediment. Geol. 470, 106719. https://doi.org/10.1016/j.sedgeo.2024.106719.
Riding, R., 1991. Classification of microbial carbonates. In: Riding, R. (Ed.), Calcareous Algae and Stromatolites. Springer-Verlag, Berlin, pp. 21–51. https://doi.org/10.1007/978-3-642-52335-9_2.
Riding, R., 2000. Microbial carbonates: the geological record of calcified bacterial–algal mats and biofilms. Sedimentology 47 (1), 179–214. https://doi.org/10.1046/j.1365-3091.2000.00003.x.
Roberts, N.M.W., Holdsworth, R.E., 2022. Timescales of faulting through calcite geochronology: a review. J. Struct. Geol. 158, 104578. https://doi.org/10.1016/j.jsg.2022.104578.
Roberts, N.M.W., Walker, R.J., 2016. U-Pb geochronology of calcite-mineralized faults: absolute timing of rift-related fault events on the Northeast Atlantic margin. Geology 44 (7), 531–534. https://doi.org/10.1130/G37868.1.
Roberts, N.M.W., Rasbury, E.T., Parrish, R.R., Smith, C.J., Horstwood, M.S., Condon, D. J., 2017. A calcite reference material for LA-ICP-MS U-Pb geochronology. Geochem. Geophys. Geosyst. 18 (7), 2807–2814. https://doi.org/10.1002/2016GC006784.
Roberts, N.M.W., Drost, K., Horstwood, M.S., Condon, D.J., Chew, D., Drake, H., Milodowski, A.E., McLean, N.M., Smye, A.J., Walker, R.J., Haslam, R., Hodson, K., Imber, J., Beaudoin, N., Lee, J.K., 2020. Laser ablation inductively coupled plasma mass spectrometry (LA-ICP-MS) U–Pb carbonate geochronology: strategies, progress, and limitations. Geochronology 2 (1), 33–61. https://doi.org/10.5194/gchron-2-33-2020.
Rocca, M., Zanchetta, S., Gasparrini, M., Mangenot, X., Berra, F., Deschamps, P., Guihou, A., Zanchi, A., 2024. U-Pb carbonate dating reveals long-lived activity of proximal margin extensional faults during the Alpine Tethys rifting. Terra Nova 36 (5), 347–357.
Rochín-Bañaga, H., Davis, D.W., Schwennicke, T., 2021. First U-Pb dating of fossilized soft tissue using a new approach to paleontological chronometry. Geology 49, 1027–1031. https://doi.org/10.1130/G48386.1.
Rochín-Bañaga, H., Davis, D.W., Moysiuk, J., 2024. U–Pb dating of belemnites and rugose corals: the potential for absolute dating of calcitic invertebrate fossils. Chem. Geol. 644, 121862. https://doi.org/10.1016/j.chemgeo.2023.121862.
Rohais, S., Hamon, Y., Deschamps, R., Beaumont, V., Gasparrini, M., Pillot, D., Romero-Sarmiento, M., 2019. Patterns of organic carbon enrichment in a lacustrine system across the K-T boundary: insight from a multi-proxy analysis of the Yacoraite Formation, Salta rift basin, Argentina. Int. J. Coal Geol. 210, 103208. https://doi.org/10.1016/j.coal.2019.05.015.
Romero-Sarmiento, M.-F., Rohais, S., Littke, R., 2019. Lacustrine type I kerogen characterization at different thermal maturity levels: application to the late cretaceous Yacoraite Formation in the Salta Basin – Argentina. Int. J. Coal Geol. 203, 15–27. https://doi.org/10.1016/j.coal.2019.01.004.
Rubidge, B.S., Erwin, D.H., Ramezani, J., Bowring, S.A., de Klerk, W.J., 2013. High-precision temporal calibration of late Permian vertebrate biostratigraphy: U-Pb zircon constraints from the Karoo Supergroup, South Africa. Geology 41, 363–366. https://doi.org/10.1130/G33622.1.
Ryan, B.H., Kaczmarek, S.E., Rivers, J.M., Manche, C.J., 2022. Extensive recrystallization of Cenozoic dolomite during shallow burial: a case study from the Palaeocene–Eocene Umm er Radhuma formation and a global meta-analysis. Sedimentology 69 (5), 2053–2079. https://doi.org/10.1111/sed.12982.
Salfity, J.A., Marquillas, R.A., 1994. Tectonic and sedimentary evolution of the Cretaceous-Eocene Salta Group Basin, Argentina. In: Salfity, J.A. (Ed.), Cretaceous Tectonics of the Andes. Earth Evolution Sciences, pp. 266–315. https://doi.org/10.1007/978-3-322-85472-8_6.
Scardia, G., Parenti, F., Miggins, D.P., Gerdes, A., Araujo, A.G., Neves, W.A., 2019. Chronologic constraints on hominin dispersal outside Africa since 2.48 Ma from the Zarqa Valley, Jordan. Quat. Sci. Rev. 219, 1–19. https://doi.org/10.1016/j.quascirev.2019.06.007.
Sellwood, B.W., Beckett, D., 1991. Ooid microfabrics: the origin and distribution of high intra-ooid porosity; Mid-Jurassic reservoirs, S. England. Sediment. Geol. 71 (3–4), 189–193. https://doi.org/10.1016/0037-0738(91)90101-I.
Sial, A., Ferreira, V., Toselli, A., Parada, M., Aceñolaza, F., Pimentel, M., Alonso, R., 2001. Carbon and oxygen isotope compositions of some Upper Cretaceous–Paleocene sequences in Argentina and Chile. Int. Geol. Rev. 43, 892–909. https://doi.org/10.1080/00206810109465054.
Singh, S.K., Dalai, T.K., Krishnaswami, S., 2003. ^{238}U series isotopes and ^{232}Th in carbonates and black shales from the Lesser Himalaya: implications to dissolved uranium abundances in Ganga-Indus source waters. J. Environ. Radioact. 67 (1), 69–90. https://doi.org/10.1016/S0265-931X(02)00161-3.
Smith, J.J., Ludvigson, G.A., Layzell, A., Möller, A., Harlow, R.H., Turner, E., Platt, B., Petronis, M., 2017. Discovery of Paleogene deposits of the central High Plains aquifer in the western Great Plains, USA. J. Sediment. Res. 87, 880–896. https://doi.org/10.2110/jsr.2017.48.
Smith, P.E., Farquhar, R.M., 1989. Direct dating of Phanerozoic sediments by the ^{238}U single bond ^{206}Pb method. Nature 341, 518–521. https://doi.org/10.1038/341518a0.
Smith, P.E., Brand, U., Farquhar, R.M., 1994. U-Pb systematics and alteration trends of Pennsylvanianaged aragonite and calcite. Geochim. Cosmochim. Acta 58, 313–322. https://doi.org/10.1016/0016-7037(94)90466-9.
Środoń, J., Gerdes, A., Kramers, J., Bojanowski, M.J., 2022. Age constraints of the Sturtian glaciation on western Baltica based on U-Pb and Ar-Ar dating of the Lapichi Svita. Precambrian Res. 371, 106595. https://doi.org/10.1016/j.precamres.2022.106595.
Sturchio, N.C., Antonio, M.R., Soderholm, L., Sutton, S.R., Brannon, J.C., 1998. Tetravalent uranium in calcite. Science 281 (5379), 971–973. https://doi.org/10.1126/science.281.5379.9.
Suarez-Gonzalez, P., Reitner, J., 2021. Ooids forming in situ within microbial mats (Kiritimati atoll, Central Pacific). PalZ 95, 809–821. https://doi.org/10.1007/s12542-021-00591-6.
Suarez-Gonzalez, P., Benito, M.I., Quijada, I.E., Mas, R., Campos-Soto, S., 2019. 'Trapping and binding': a review of the factors controlling the development of fossil agglutinated microbialites and their distribution in space and time. Earth Sci. Rev. 194, 182–215. https://doi.org/10.1016/j.earscirev.2019.05.007.
Summons, R.E., Bird, L.R., Gillespie, A.L., Pruss, S.B., Roberts, M., Sessions, A.L., 2013. Lipid biomarkers in ooids from different locations and ages: evidence for a common bacterial flora. Geobiology 11 (5), 420–436. https://doi.org/10.1111/gbi.12047.
Sumner, D.Y., Grotzinger, J.P., 1993. Numerical modeling of ooid size and the problem of Neoproterozoic giant ooids. J. Sediment. Petrol. 63 (5), 974–982. https://doi.org/10.1306/D4267C5D-2B26-11D7-8648000102C1865D.
Taylor, S.R., McLennan, S.M., 1985. The Continental Crust: Its Composition and Evolution. Blackwell Scientific Publications, Oxford, p. 312.
Teles, V., Hamon, Y., Deschamps, R., Rohais, S., Nader, F.H., Heckenmeyer, E., Gasparrini, M., Barbier, M., Lerat, O., Joseph, P., Doligez, B., 2023. Modelling the coupled heterogeneities of the lacustrine microbialite-bearing carbonate reservoir of the Yacoraite Formation (Salta, Argentina). Comptes Rendus. Géoscience 355 (S1), 1–20. https://doi.org/10.5802/crgeos.187.
Tribovillard, N., Algeo, T.J., Lyons, T., Riboulleau, A., 2006. Trace metals as paleoredox and paleoproductivity proxies; an update. Chem. Geol. 232 (1–2), 12–32. https://doi.org/10.1016/j.chemgeo.2006.02.012.
Tucker, M.E., Wright, V.P., 1990. Carbonate Sedimentology. Blackwell, Oxford. https://doi.org/10.1002/9781444314175, 486 p.
Vanorio, T., Dvorkin, J., Mavko, G., 2009. The effect of micrite content on porosity, permeability, and acoustic velocity of carbonate rocks. In: European Association of Geoscientists & Engineers. 71st EAGE Conference and Exhibition, cp-129-00054. https://doi.org/10.3997/2214-4609.201404935.

Villafañe, P.G., Frías-Saba, R. del C., Della Vedova, M., Citton, P., Díaz-Martínez, I., de Valais, S., Aceñolaza, F.G., Marquillas, R.A., Cónsole-Gonella, C., 2022. Microbialitic deposits of the Yacoraite Formation, NW Argentina: distribution, environments, paleoecology, and economic implications. Braz. J. Geol. 52 (2). https://doi.org/10.1590/2317-4889202220210088.

Vincent, B., Rigollet, C., Cochard, J., Khalil, S., Mejia-Duran, A.F., Grégoire, D., Beaudoin, N., Brigaud, B., Blaise, T., Reuschle, T., Pellenard, P., Landrein, P., 2025. Multi-stage micrite diagenesis in the late Jurassic of the Eastern Paris Basin: petrophysical and mechanical properties for engineering purposes. Geol. Soc. Lond. Spec. Publ. 548, 311–339. https://doi.org/10.1144/sp548-2023-139.

Walter, B.F., Gerdes, A., Kleinhanns, I.C., Dunkl, I., Eynatten, H.V., Kreissl, S., Markl, G., 2018. The connection between hydrothermal fluids, mineralization, tectonics and magmatism in a continental rift setting: Fluorite Sm-Nd and hematite and carbonates U-Pb geochronology from the Rhinegraben in SW Germany. Geochim. Cosmochim. Acta 240, 11–42. https://doi.org/10.1016/j.gca.2018.08.012.

Watson, E., Swindles, G., Lawson, I., Savov, I., Wastegård, S., 2017. The presence of Holocene cryptotephra in Wales and southern England. J. Quat. Sci. https://doi.org/10.1002/jqs.2942.

Wingender, J., Neu, T.R., Flemming, H.C., 1999. Microbial Extracellular Polymeric Substances. Springer-Verlag, Berlin, 251 p.

Woodhead, J., Petrus, J.A., 2019. Exploring the advantages and limitations of in situ U-Pb carbonate geochronology using speleothems. Geochronology 1 (1), 69–84. https://doi.org/10.5194/gchron-1-69-2019.

Yang, P., Liu, K., Li, Z., Rankenburg, K., McInnes, B.I.A., Liu, J., Evans, N.J., 2022. Direct dating Paleo-fluid flow events in sedimentary basins. Chem. Geol. 588. https://doi.org/10.1016/j.chemgeo.2021.120642.

Zhao, M., Zheng, Y., 2014. Marine carbonate records of terrigenous input into Paleotethyan seawater: Geochemical constraints from Carboniferous limestones. Geochim. Cosmochim. Acta 141, 508–531. https://doi.org/10.1016/j.gca.2014.07.001.